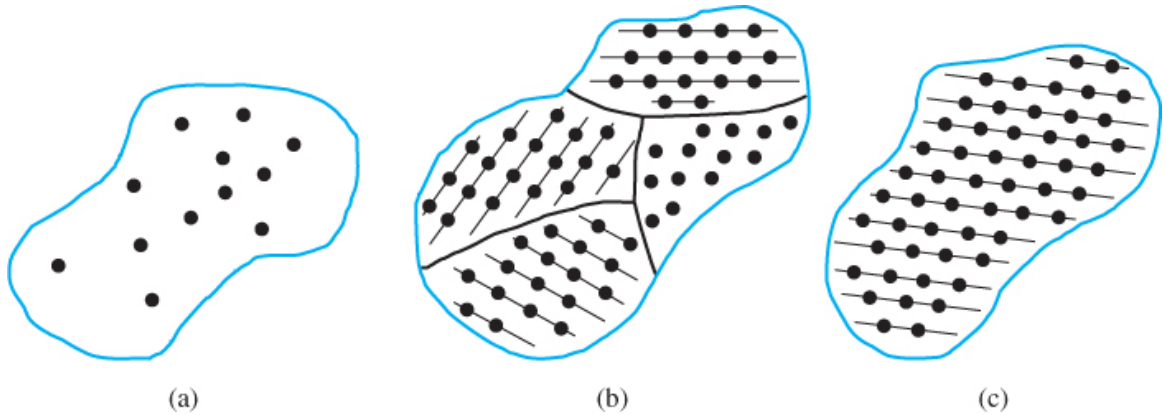

Figure 1.1 | Schematics of three general types of crystals: (a) amorphous, (b) polycrystalline, (c) single.

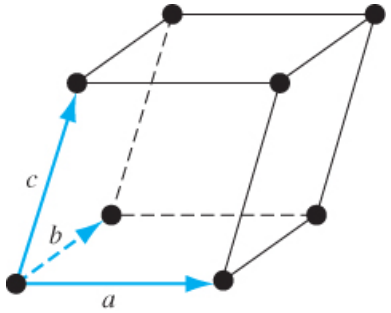

Figure 1.4 | A generalized primitive unit cell.

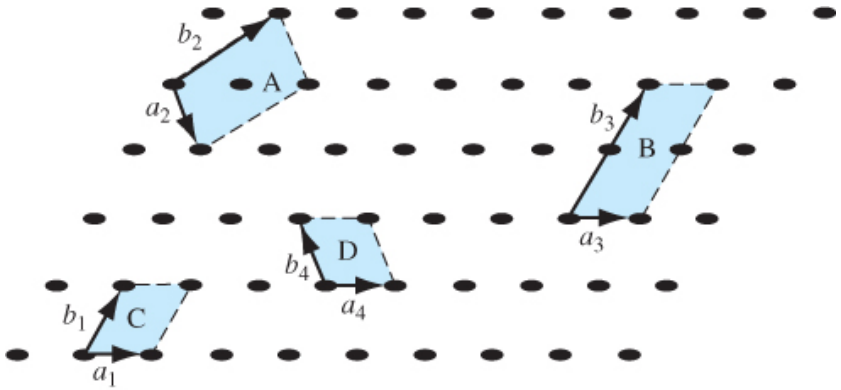

Figure 1.3 | Two-dimensional representation of a single-crystal lattice showing various possible unit cells.

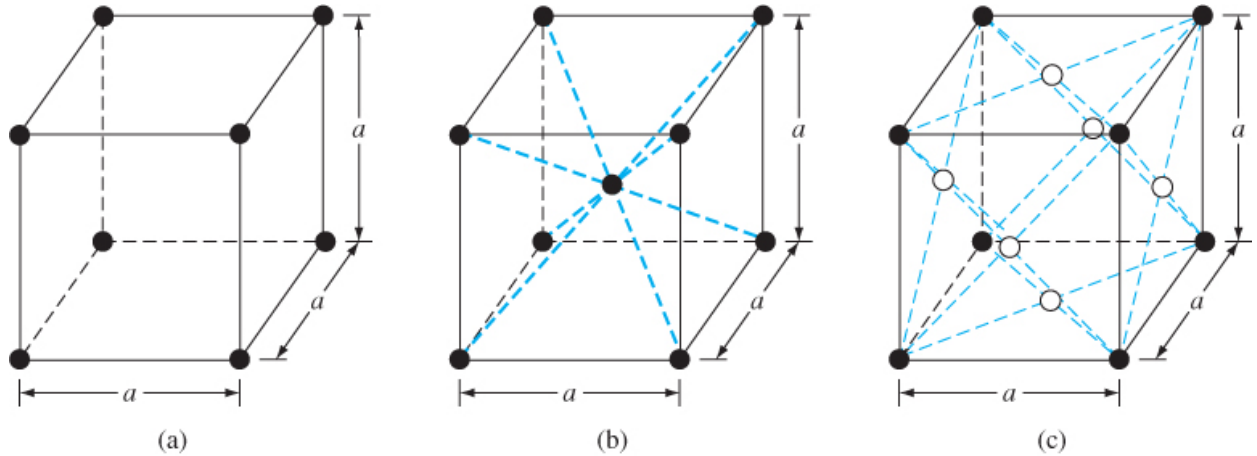

Figure 1.5 | Three lattice types: (a) simple cubic, (b) body-centered cubic, (c) face-centered cubic.

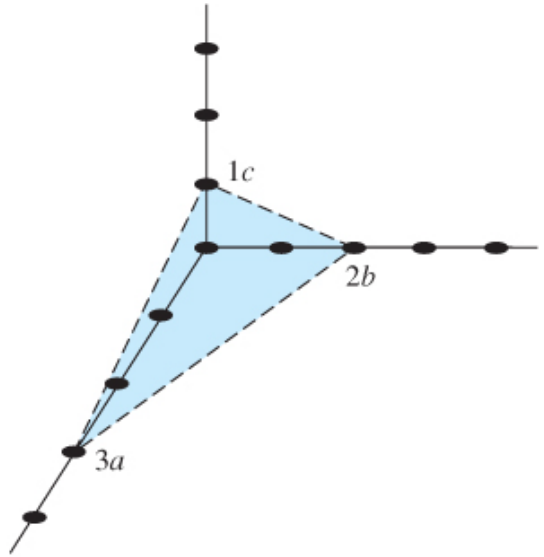

Figure 1.6 | A representative crystal-lattice plane.

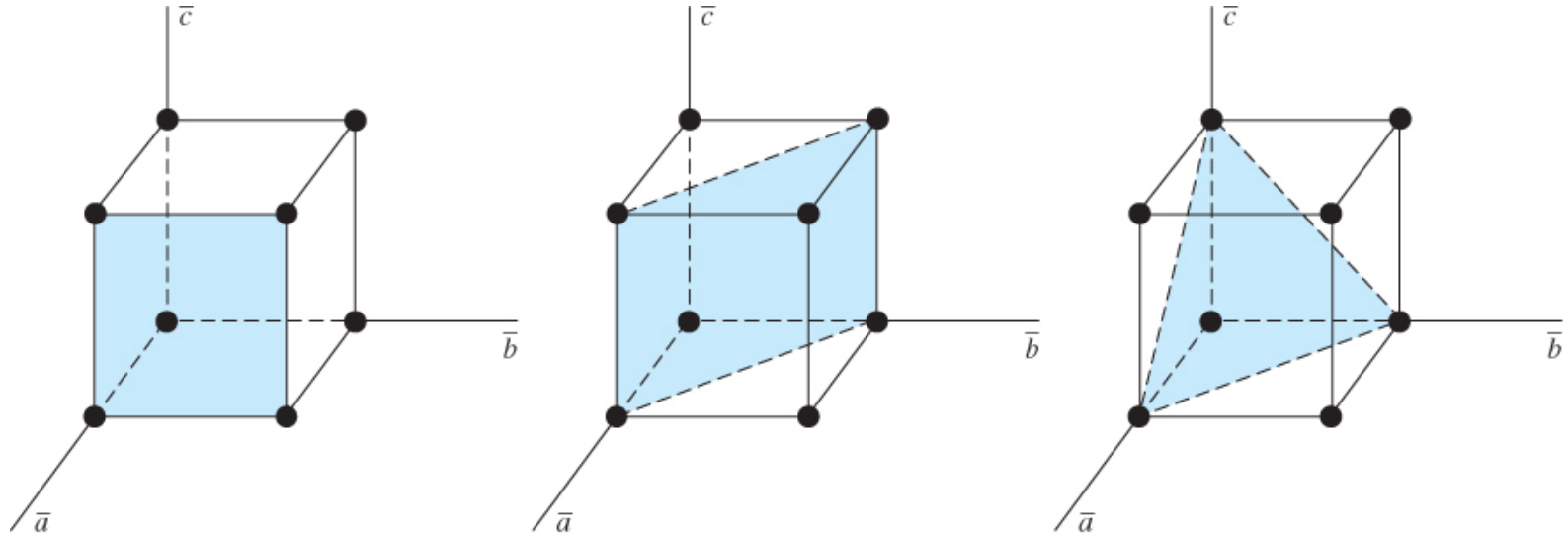

Figure 1.8 | Three lattice planes: (a) (100) plane, (b) (110) plane, (c) (111) plane.

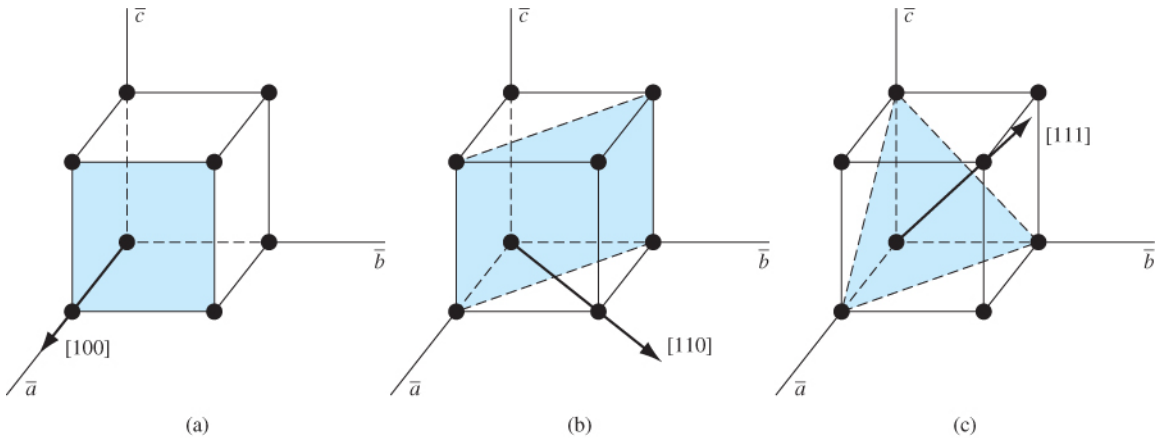

Figure 1.10 | Three lattice directions and planes: (a) (100) plane and [100] direction, (b) (110) plane and [110] direction, (c) (111) plane and [111] direction.

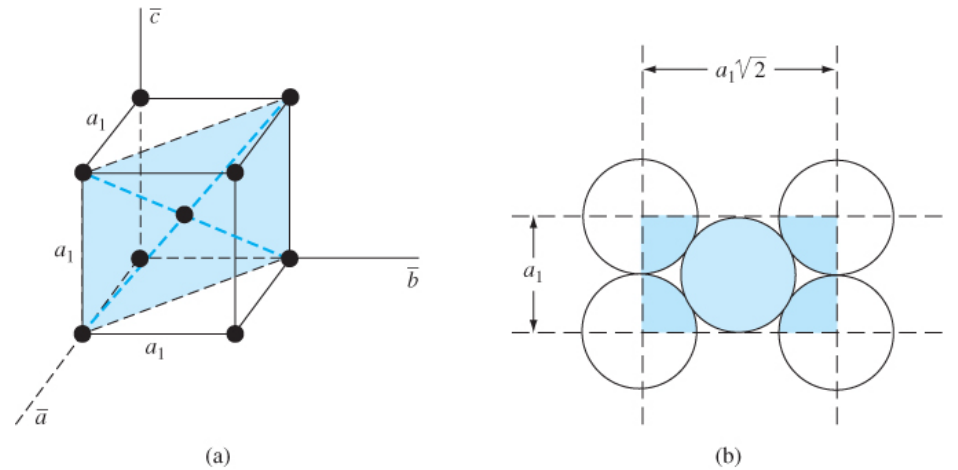

Figure 1.9 | (a) The (110) plane in a body-centered cubic and (b) the atoms cut by the (110) plane in a body-centered cubic.

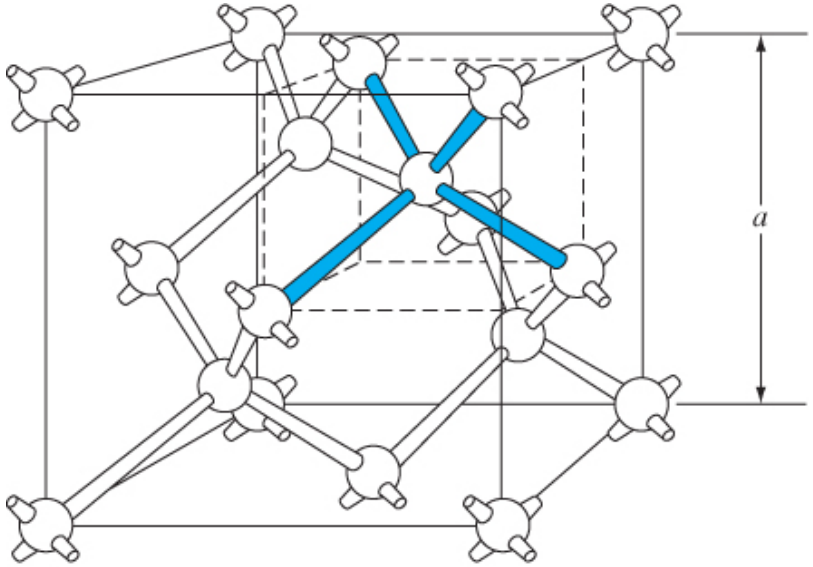

Figure 1.11 | The diamond structure.

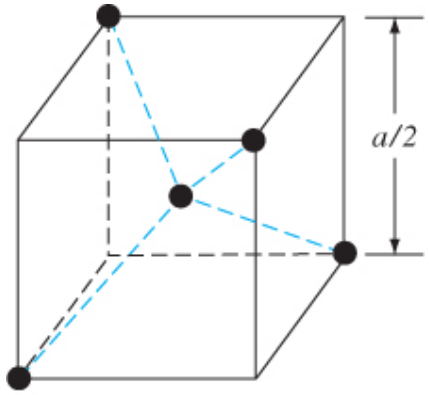

Figure 1.12 | The tetrahedral structure of closest neighbors in the diamond lattice.

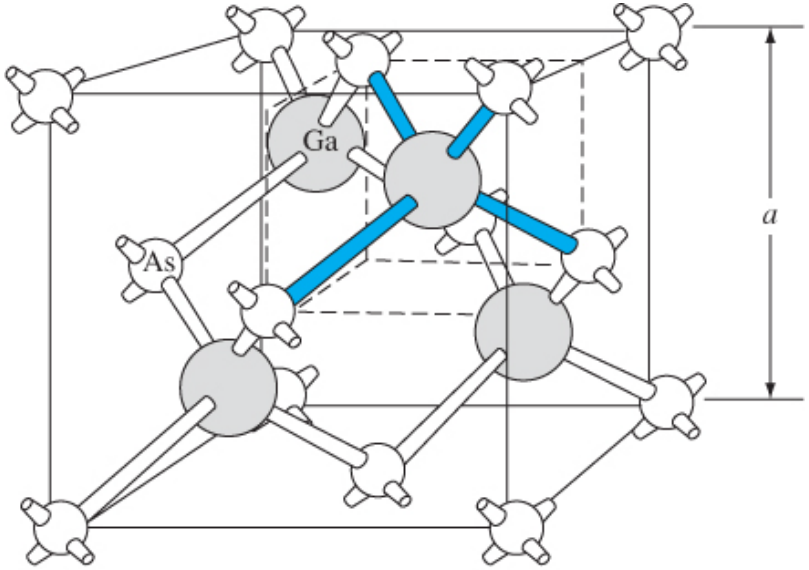

Figure 1.14 | The zincblende (sphalerite) lattice of GaAs.

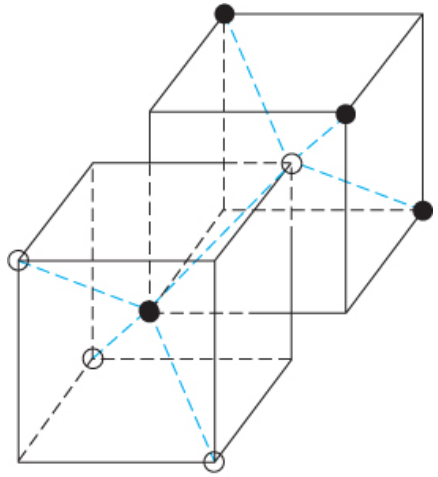

Figure 1.15 | The tetrahedral structure of closest neighbors in the zincblende lattice.

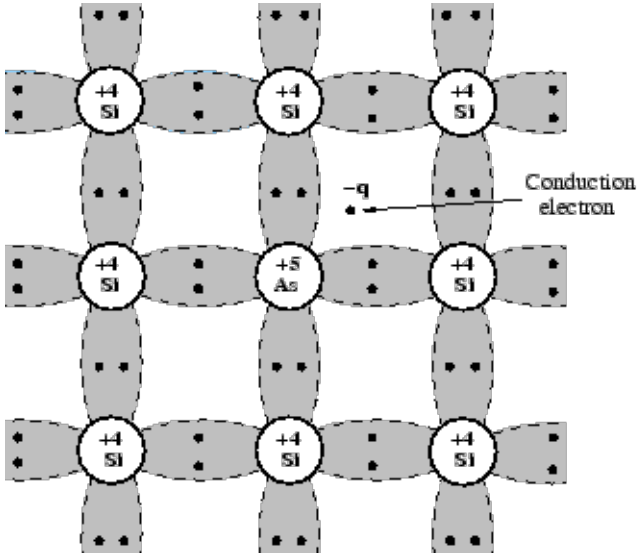
+4 Si
+5 As
−q
Conduction electron

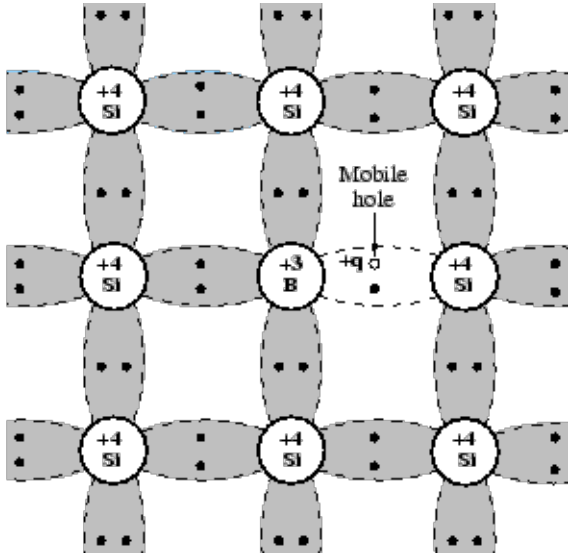
+4 Si
+3 B
Mobile hole
+q

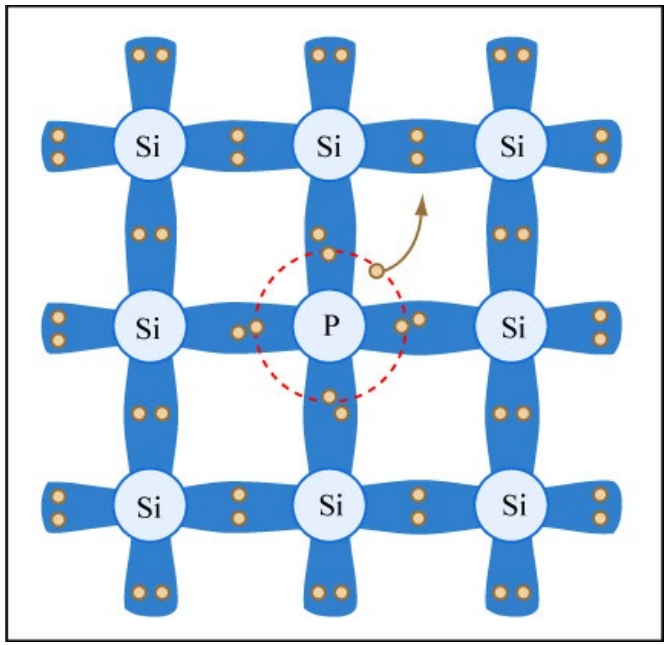
Si
P

n-Si

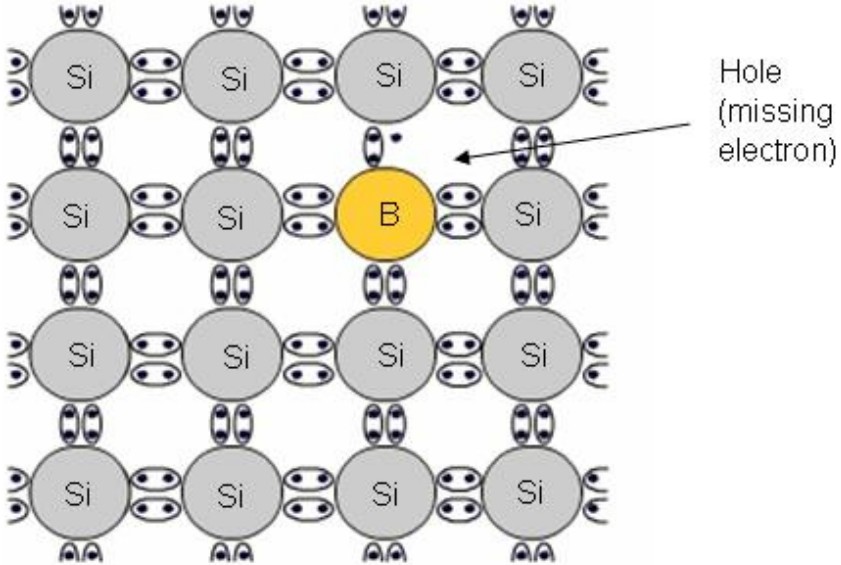
Si
B
Hole (missing electron)

p-Si

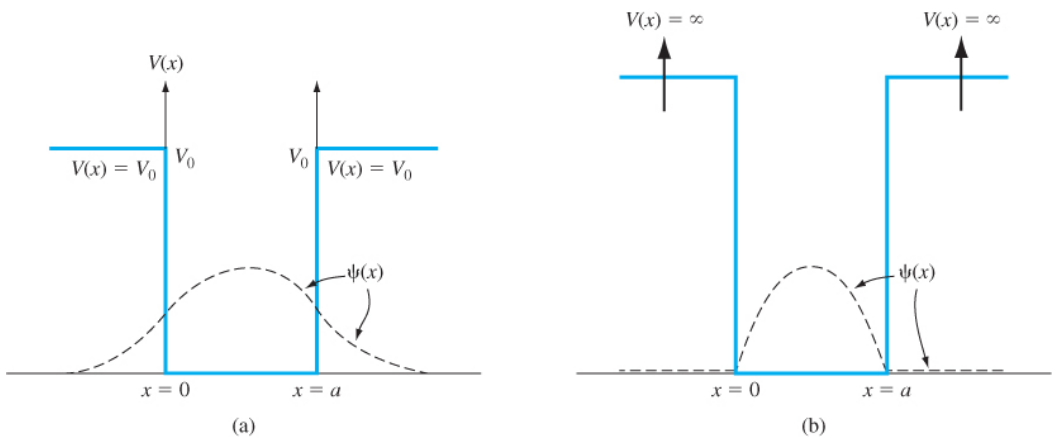

Figure 2.5 | Potential functions and corresponding wave function solutions for the case (a) when the potential function is finite everywhere and (b) when the potential function is infinite in some regions.

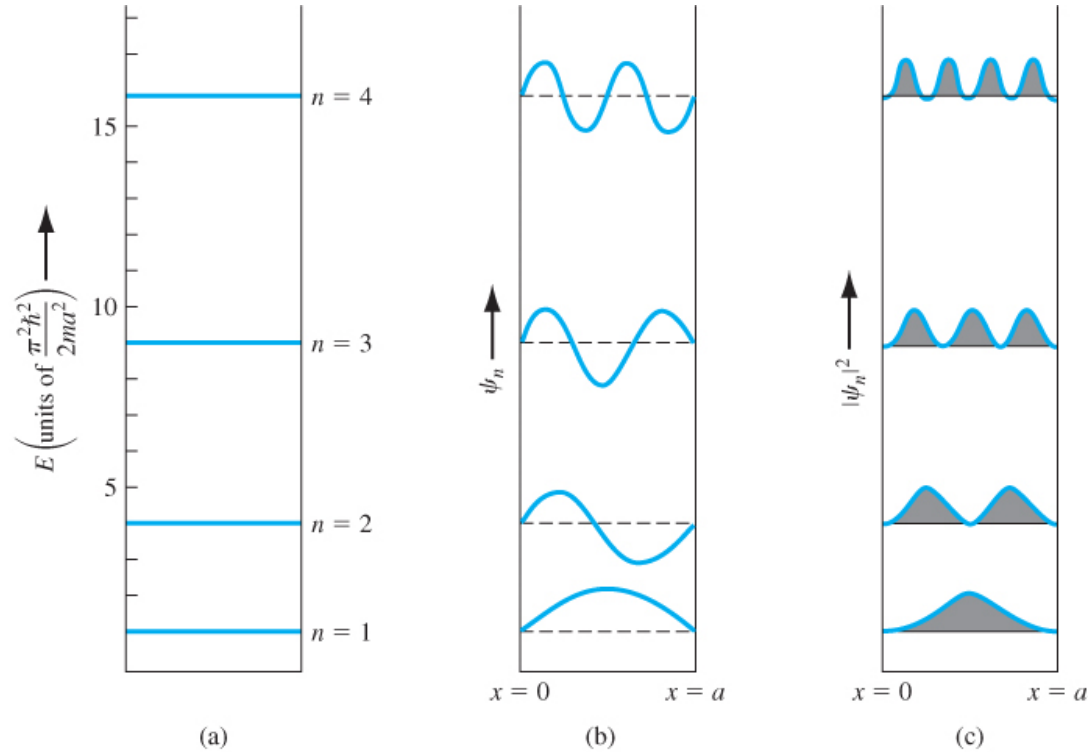

Figure 2.7 | Particle in an infinite potential well: (a) four lowest discrete energy levels, (b) corresponding wave functions, and (c) corresponding probability functions. *(From Pierret [10].)*

Table 2.1 | Initial portion of the periodic table

Element	Notation	n	l	m	s
Hydrogen	$1s^1$	1	0	0	$+\frac{1}{2}$ or $-\frac{1}{2}$
Helium	$1s^2$	1	0	0	$+\frac{1}{2}$ and $-\frac{1}{2}$
Lithium	$1s^22s^1$	2	0	0	$+\frac{1}{2}$ or $-\frac{1}{2}$
Beryllium	$1s^22s^2$	2	0	0	$+\frac{1}{2}$ and $-\frac{1}{2}$
Boron	$1s^22s^22p^1$	2	1		
Carbon	$1s^22s^22p^2$	2	1		
Nitrogen	$1s^22s^22p^3$	2	1		$m = 0, -1, +1$
Oxygen	$1s^22s^22p^4$	2	1		$s = +\frac{1}{2}, -\frac{1}{2}$
Fluorine	$1s^22s^22p^5$	2	1		
Neon	$1s^22s^22p^6$	2	1		

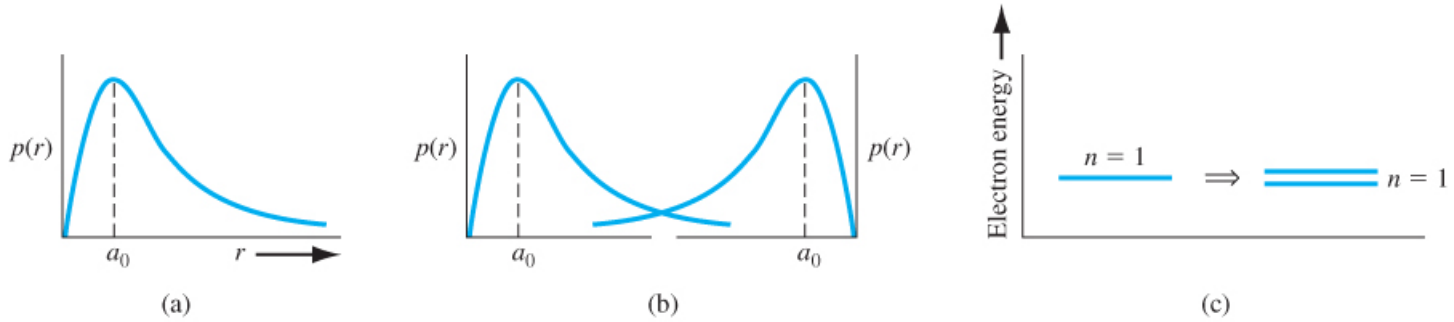

Figure 3.1 | (a) Probability density function of an isolated hydrogen atom. (b) Overlapping probability density functions of two adjacent hydrogen atoms. (c) The splitting of the $n = 1$ state.

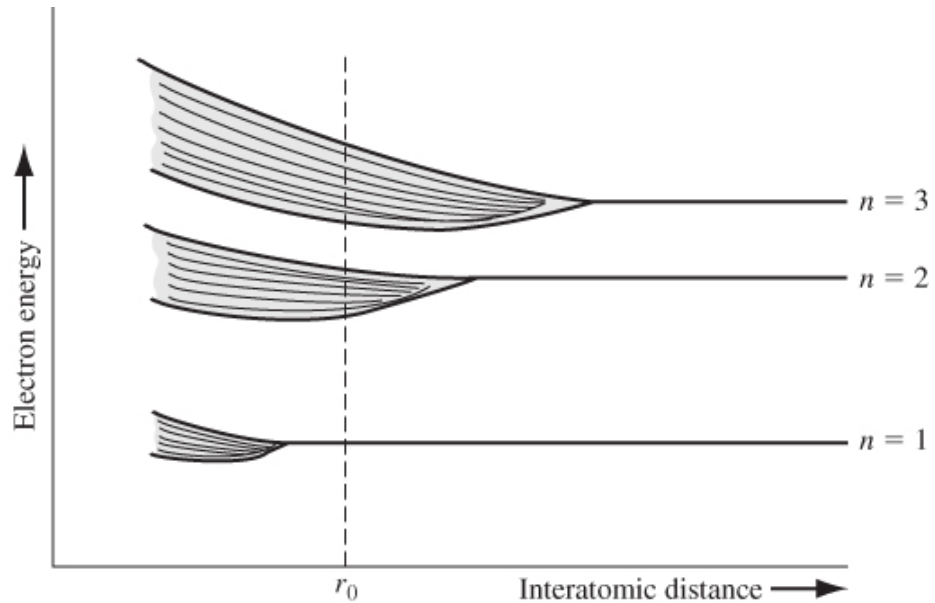

Figure 3.3 | Schematic showing the splitting of three energy states into allowed bands of energies.

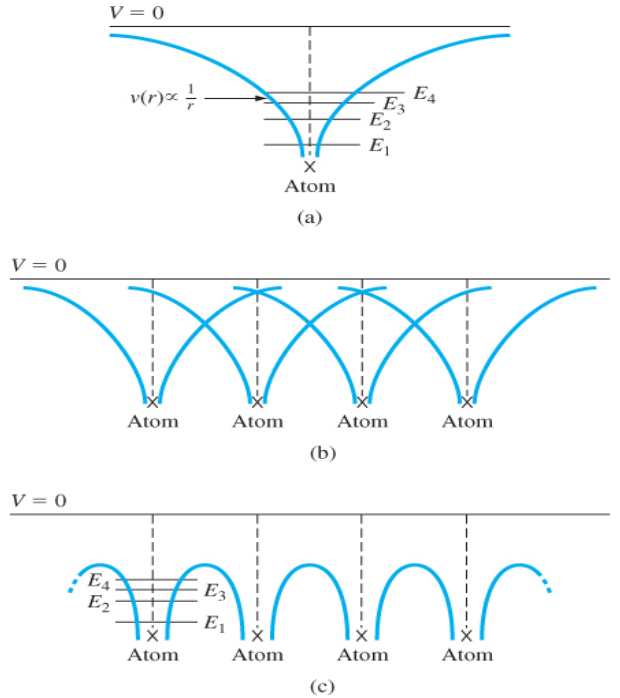

Figure 3.5 | (a) Potential function of a single isolated atom. (b) Overlapping potential functions of adjacent atoms. (c) Net potential function of a one-dimensional single crystal.

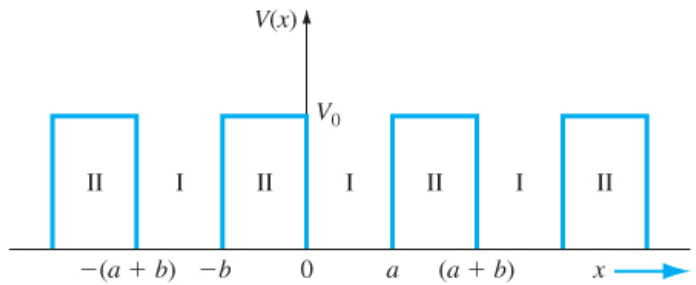

Figure 3.6 | The one-dimensional periodic potential function of the Kronig–Penney model.

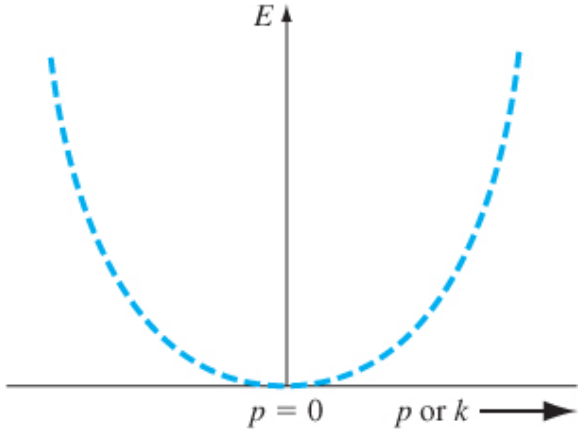

Figure 3.7 | The parabolic E versus k curve for the free electron.

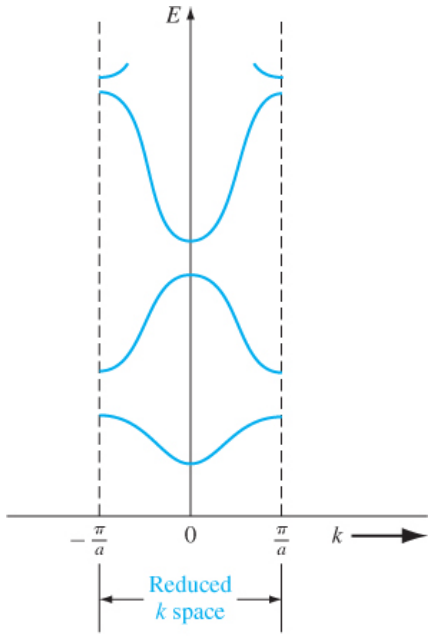

Figure 3.11 | The E versus k diagram in the reduced-zone representation.

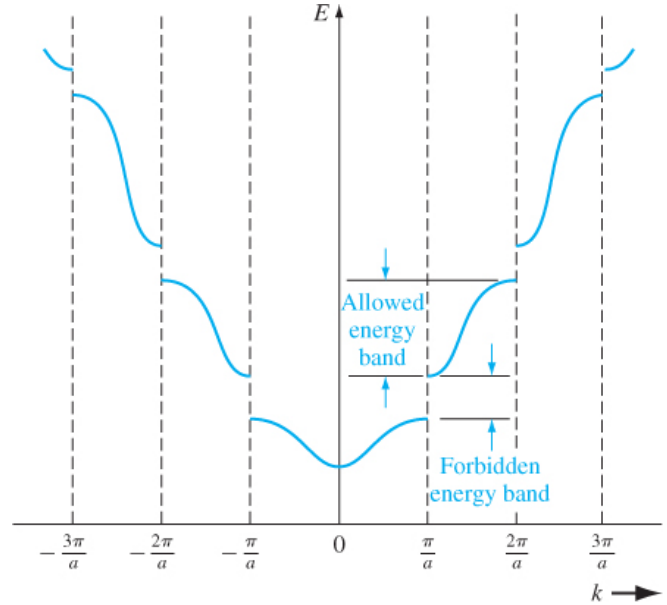

Figure 3.9 | The E versus k diagram generated from Figure 3.8. The allowed energy bands and forbidden energy bandgaps are indicated.

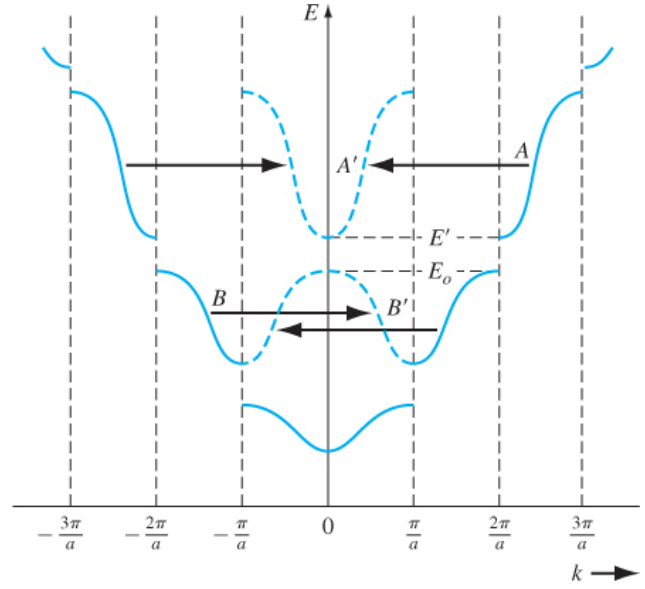

Figure 3.10 | The E versus k diagram showing 2π displacements of several sections of allowed energy bands.

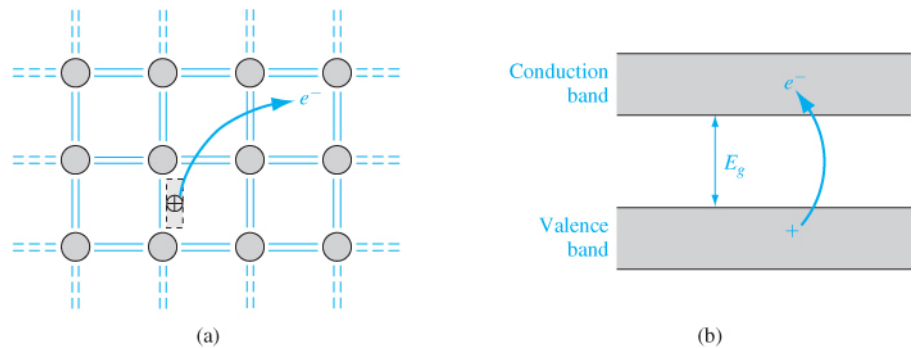

Figure 3.13 | (a) Two-dimensional representation of the breaking of a covalent bond. (b) Corresponding line representation of the energy band and the generation of a negative and positive charge with the breaking of a covalent bond.

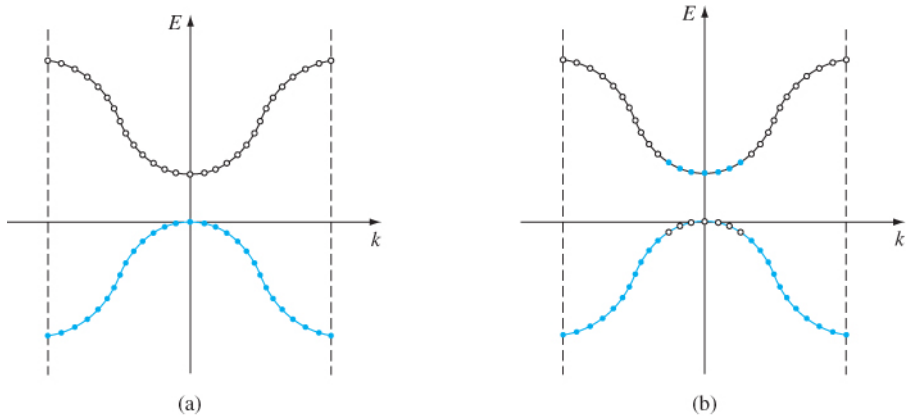

Figure 3.14 | The E versus k diagram of the conduction and valence bands of a semiconductor at (a) $T = 0$ K and (b) $T > 0$ K.

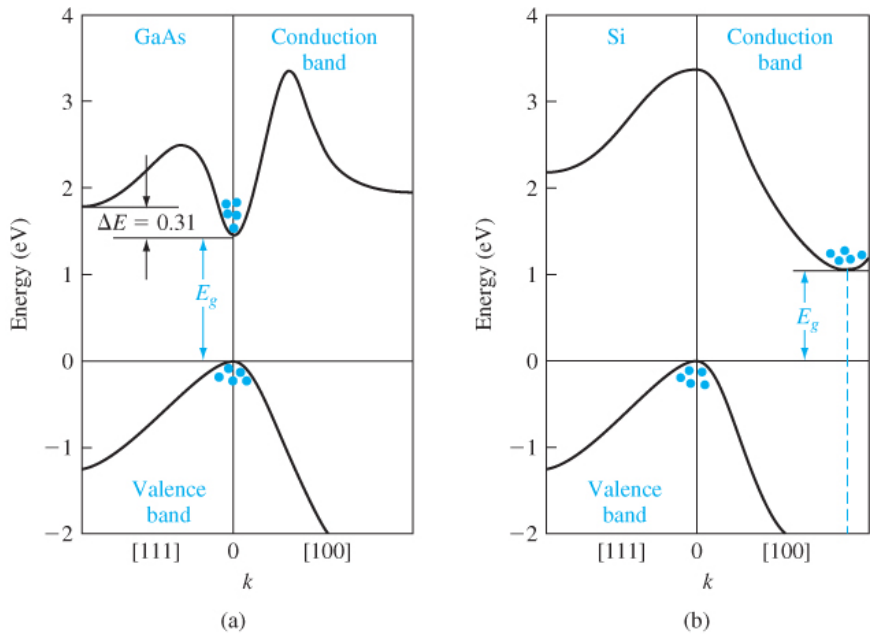

Figure 3.25 | Energy-band structures of (a) GaAs and (b) Si. *(From Sze [12].)*

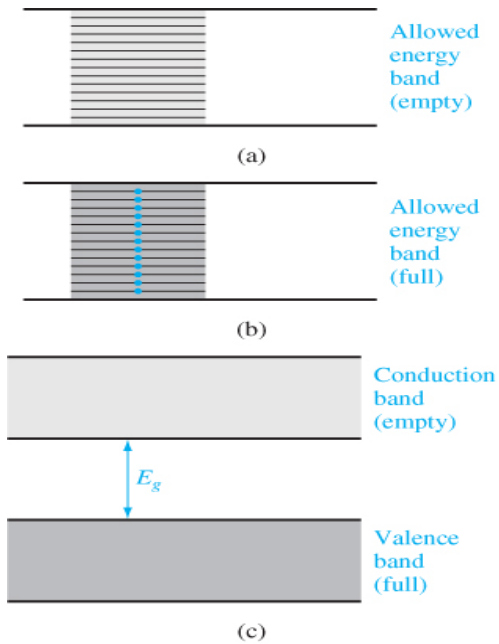

Figure 3.19 | Allowed energy bands showing (a) an empty band, (b) a completely full band, and (c) the bandgap energy between the two allowed bands.

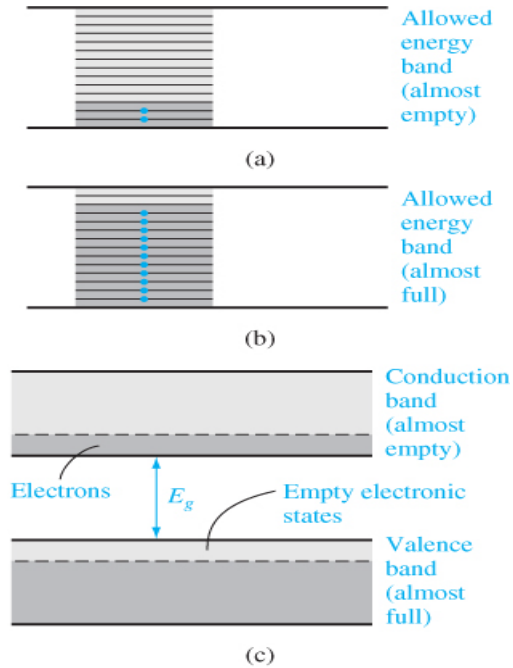

Figure 3.20 | Allowed energy bands showing (a) an almost empty band, (b) an almost full band, and (c) the bandgap energy between the two allowed bands.

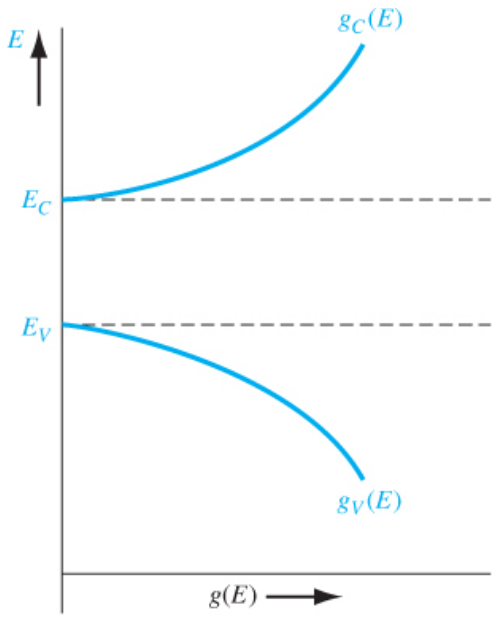

Figure 3.27 | The density of energy states in the conduction band and the density of energy states in the valence band as a function of energy.

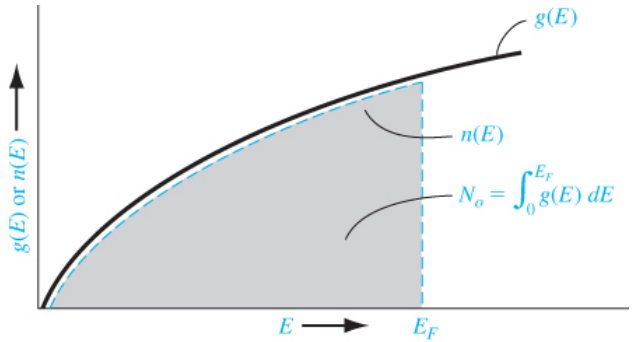

Figure 3.31 | Density of quantum states and electrons in a continuous energy system at $T = 0$ K.

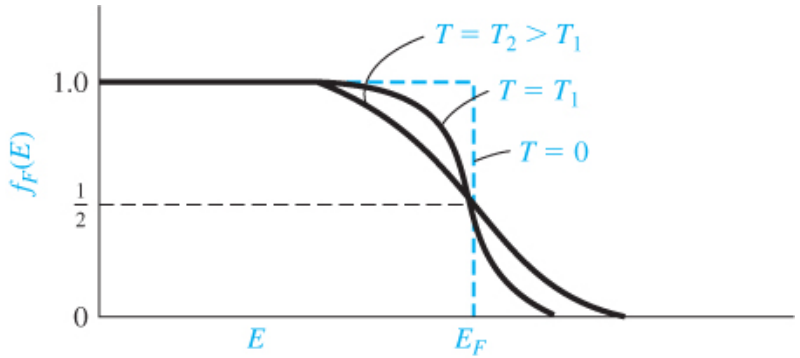

Figure 3.33 | The Fermi probability function versus energy for different temperatures.

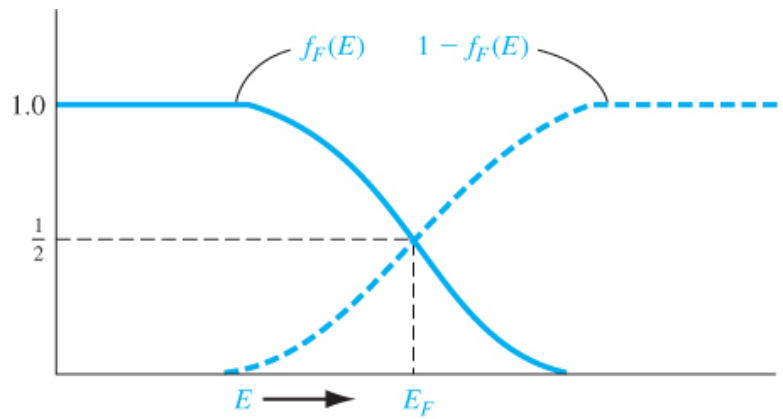

Figure 3.34 | The probability of a state being occupied, $f_F(E)$, and the probability of a state being empty, $1 - f_F(E)$.

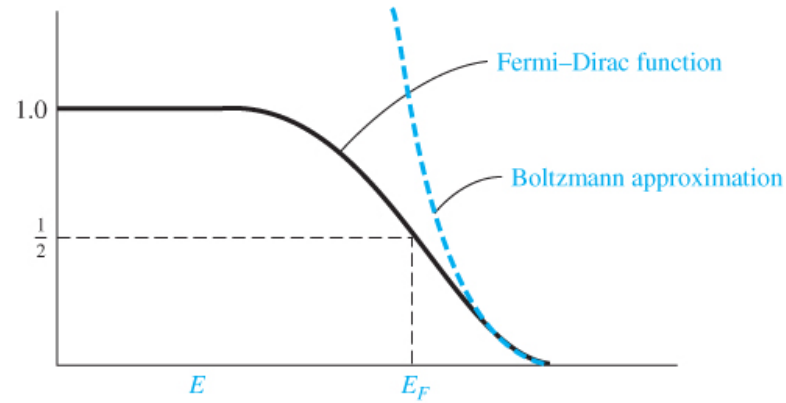

Figure 3.35 | The Fermi–Dirac probability function and the Maxwell–Boltzmann approximation.

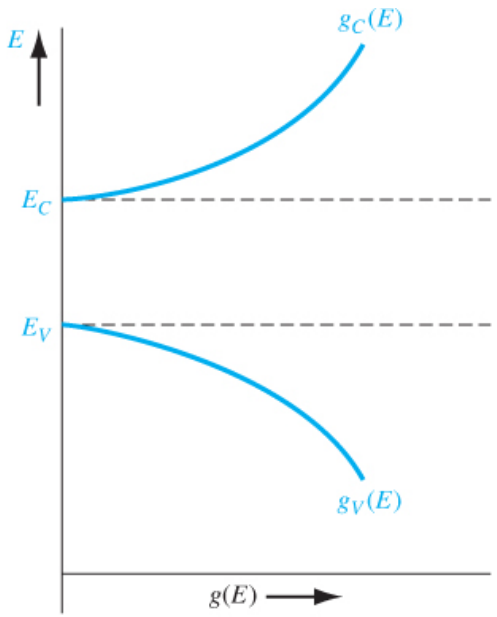

Figure 3.27 | The density of energy states in the conduction band and the density of energy states in the valence band as a function of energy.

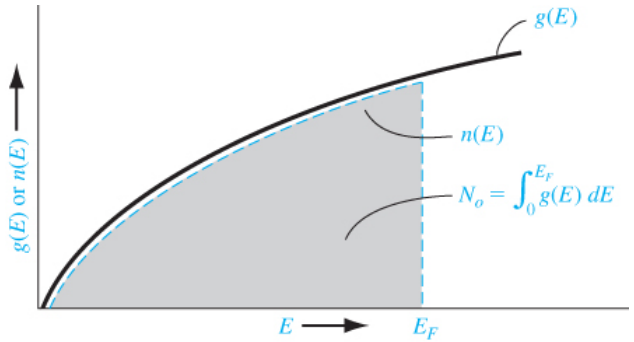

Figure 3.31 | Density of quantum states and electrons in a continuous energy system at $T = 0$ K.

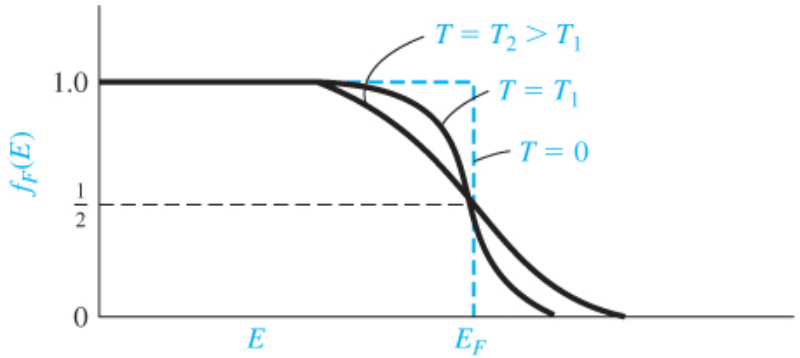

Figure 3.33 | The Fermi probability function versus energy for different temperatures.

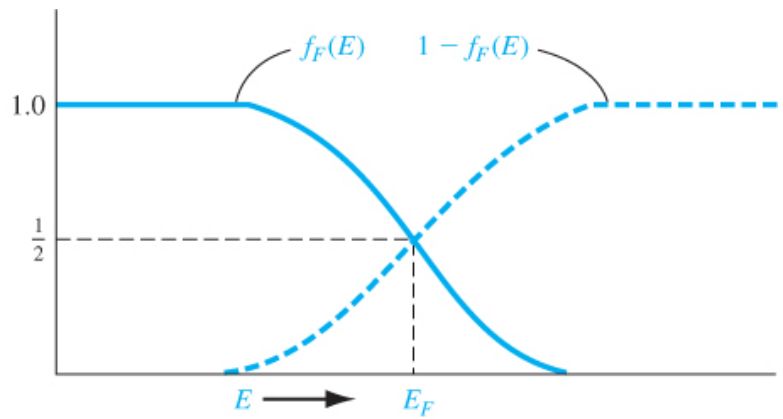

Figure 3.34 | The probability of a state being occupied, $f_F(E)$, and the probability of a state being empty, $1 - f_F(E)$.

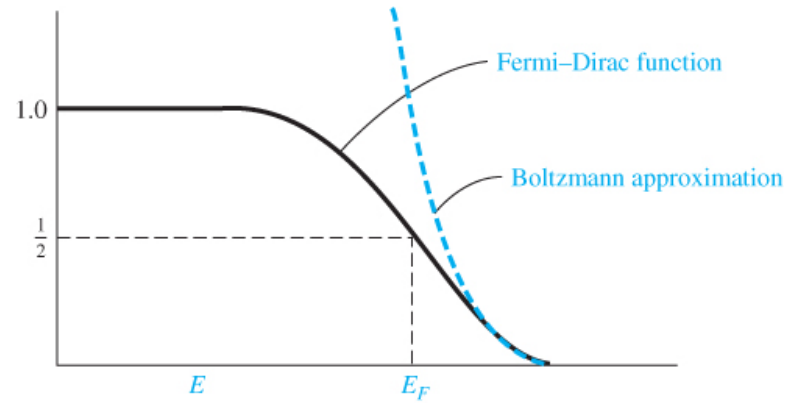

Figure 3.35 | The Fermi–Dirac probability function and the Maxwell–Boltzmann approximation.

Table 4.2 | Commonly accepted values of n_i at $T = 300$ K

Silicon	$n_i = 1.5 \times 10^{10}$ cm^{-3}
Gallium arsenide	$n_i = 1.8 \times 10^{6}$ cm^{-3}
Germanium	$n_i = 2.4 \times 10^{13}$ cm^{-3}

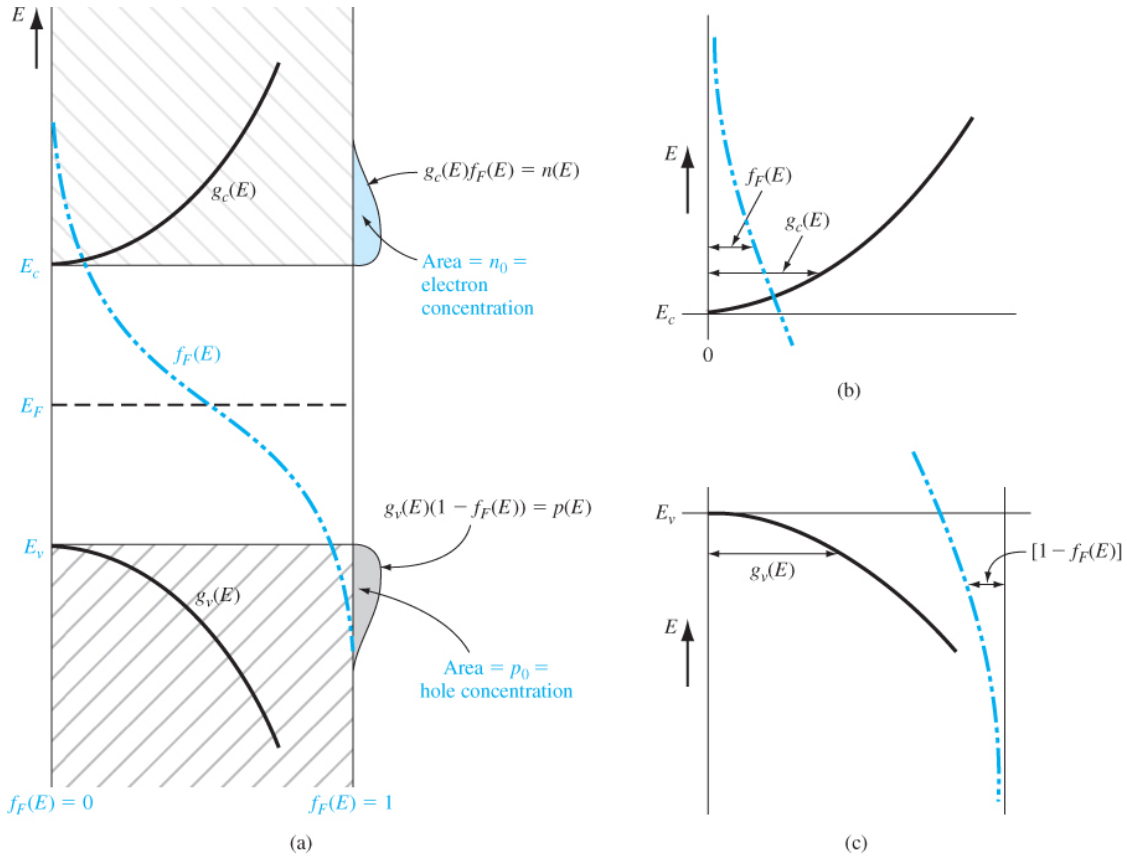

Figure 4.1 | (a) Density of states functions, Fermi–Dirac probability function, and areas representing electron and hole concentrations for the case when E_F is near the midgap energy; (b) expanded view near the conduction-band energy; and (c) expanded view near the valence-band energy.

Table 4.4 | Impurity ionization energies in gallium arsenide

Impurity	Ionization energy (eV)
Donors	
Selenium	0.0059
Tellurium	0.0058
Silicon	0.0058
Germanium	0.0061
Acceptors	
Beryllium	0.028
Zinc	0.0307
Cadmium	0.0347
Silicon	0.0345
Germanium	0.0404

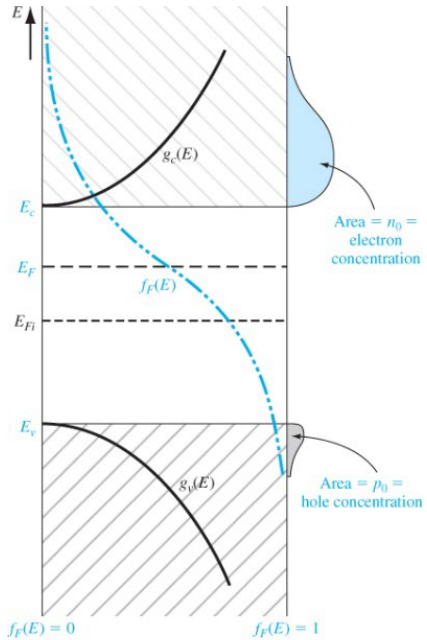

Figure 4.8 | Density of states functions, Fermi–Dirac probability function, and areas representing electron and hole concentrations for the case when E_F is above the intrinsic Fermi energy.

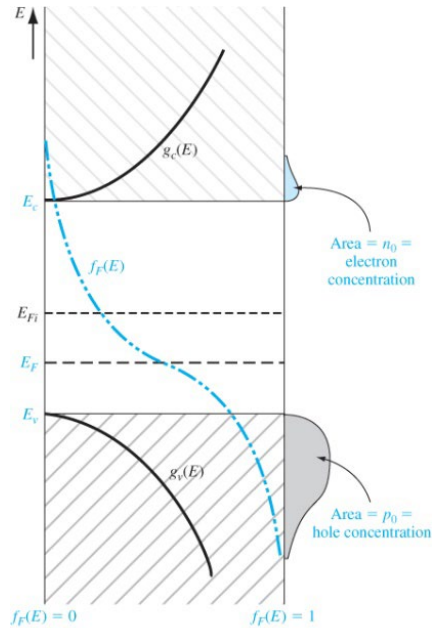

Figure 4.9 | Density of states functions, Fermi–Dirac probability function, and areas representing electron and hole concentrations for the case when E_F is below the intrinsic Fermi energy.

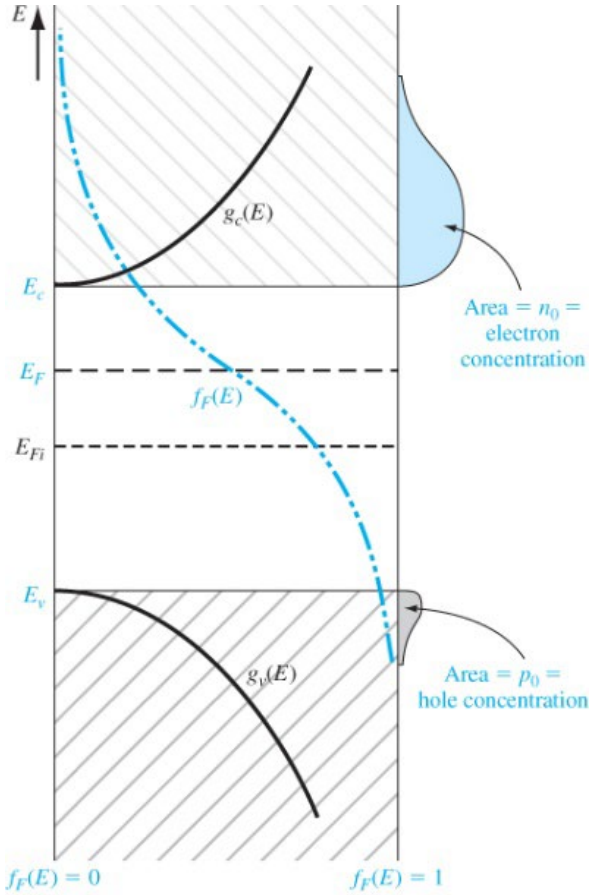

Figure 4.8 | Density of states functions, Fermi–Dirac probability function, and areas representing electron and hole concentrations for the case when E_F is above the intrinsic Fermi energy.

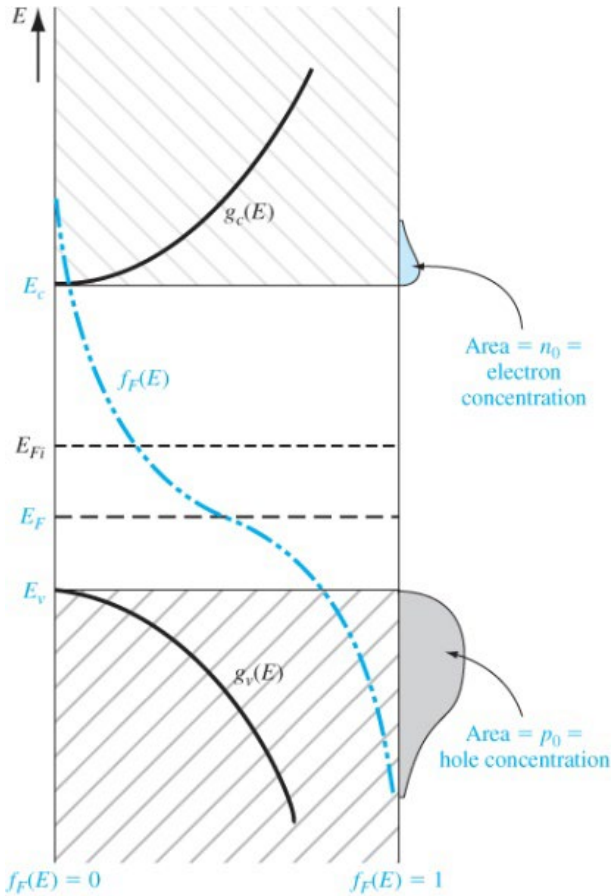

Figure 4.9 | Density of states functions, Fermi–Dirac probability function, and areas representing electron and hole concentrations for the case when E_F is below the intrinsic Fermi energy.

Table 4.4 | Impurity ionization energies in gallium arsenide

Impurity	Ionization energy (eV)
Donors	
Selenium	0.0059
Tellurium	0.0058
Silicon	0.0058
Germanium	0.0061
Acceptors	
Beryllium	0.028
Zinc	0.0307
Cadmium	0.0347
Silicon	0.0345
Germanium	0.0404

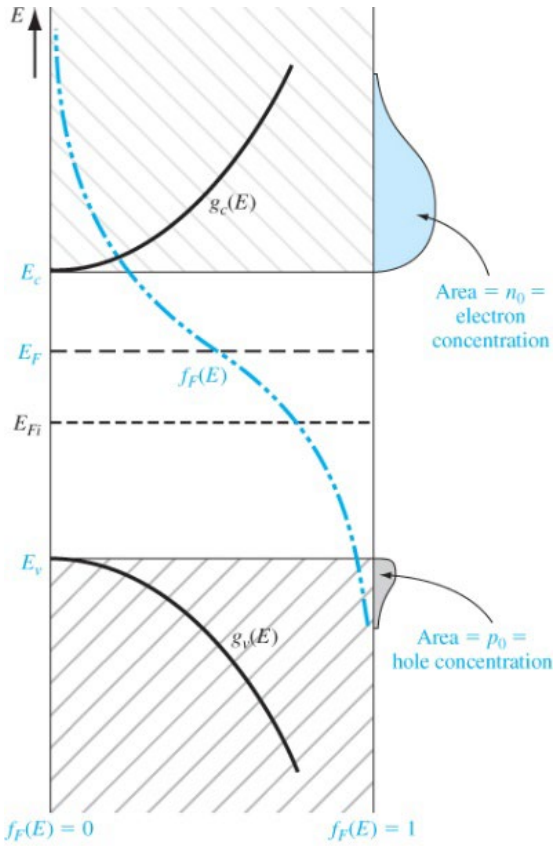

Figure 4.8 | Density of states functions, Fermi–Dirac probability function, and areas representing electron and hole concentrations for the case when E_F is above the intrinsic Fermi energy.

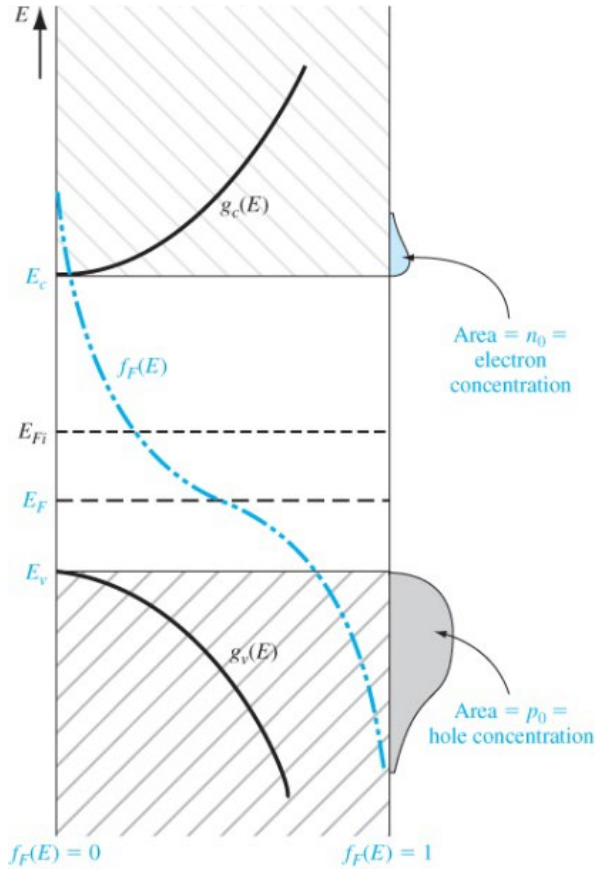

Figure 4.9 | Density of states functions, Fermi–Dirac probability function, and areas representing electron and hole concentrations for the case when E_F is below the intrinsic Fermi energy.

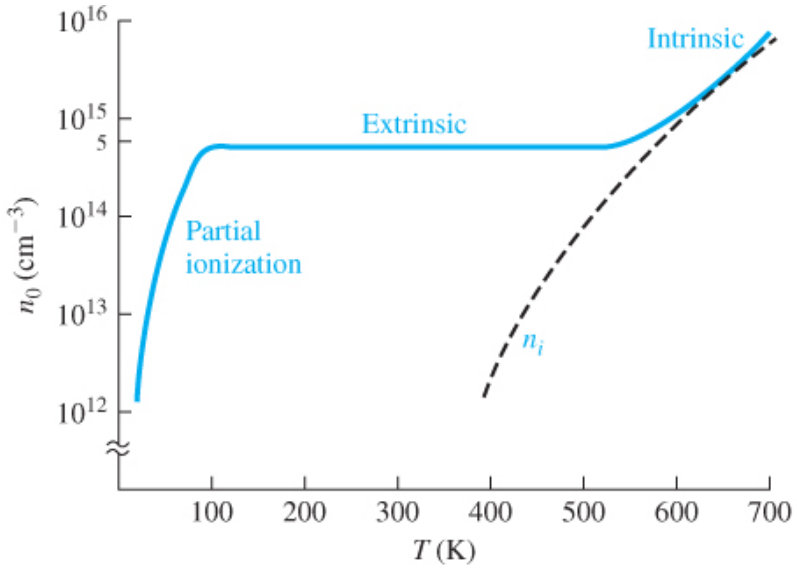

Figure 4.16 | Electron concentration versus temperature showing the three regions: partial ionization, extrinsic, and intrinsic.

Heterojunctions (p.354)

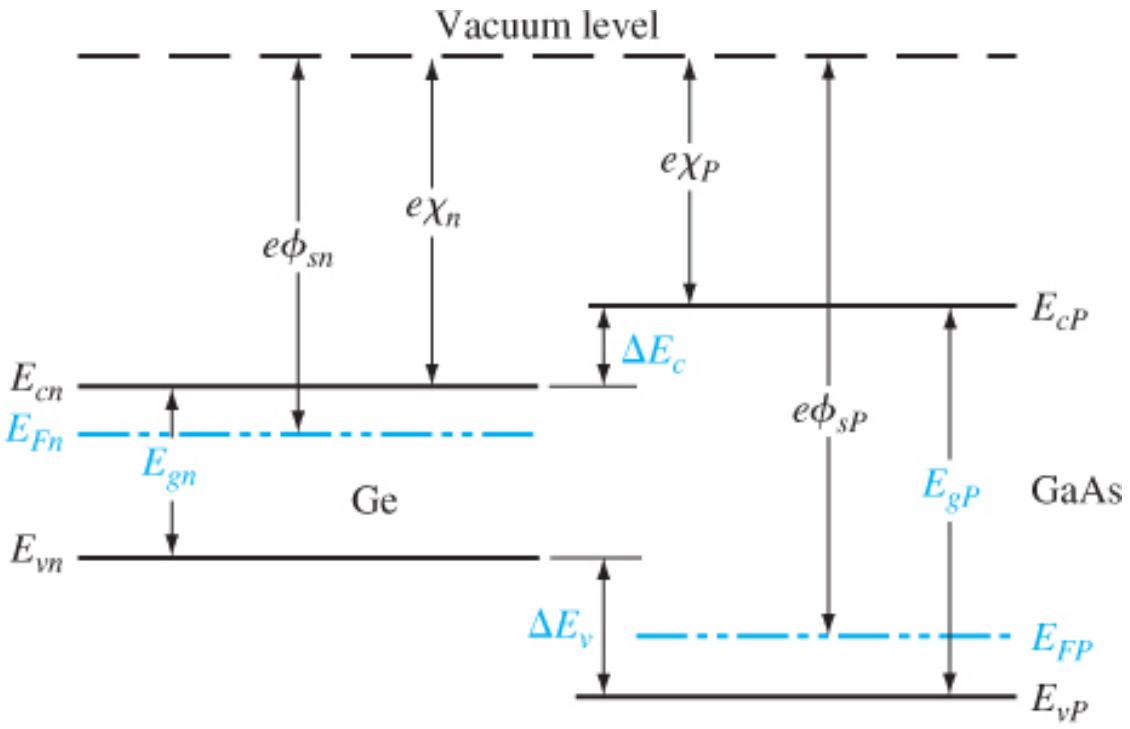

Figure 9.17 | Energy-band diagrams of a narrow-bandgap and a wide-bandgap material before contact.

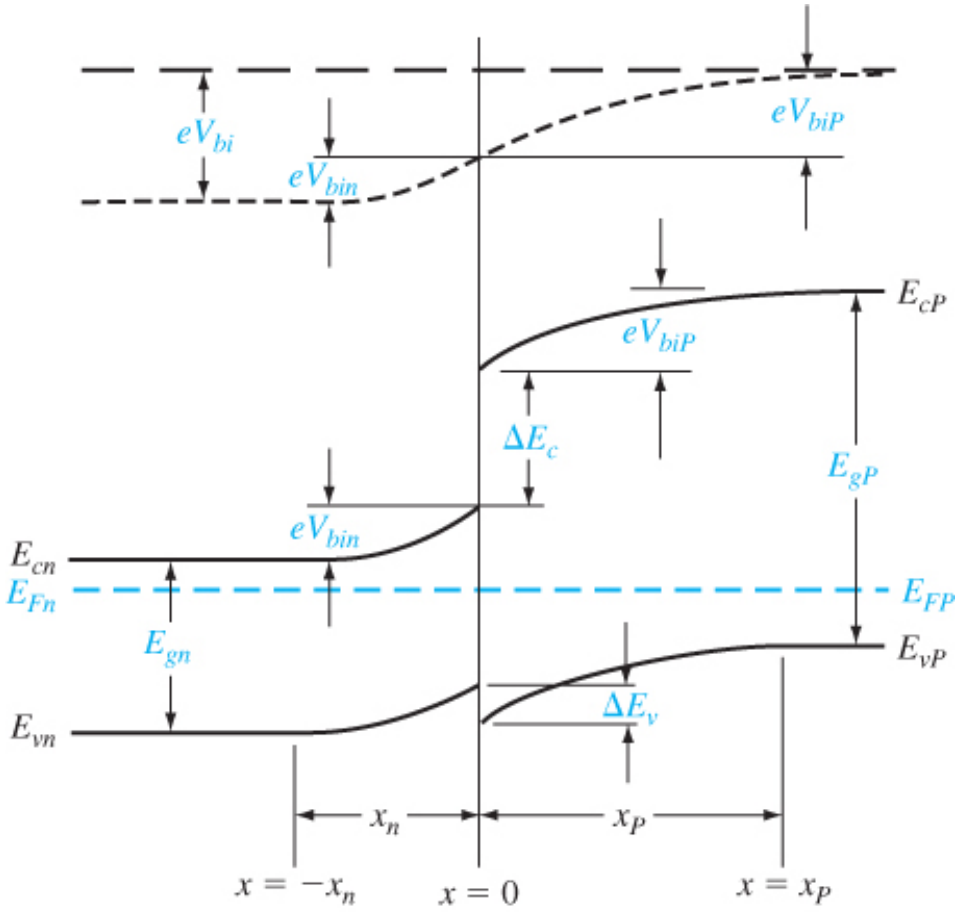

Figure 9.18 | Ideal energy-band diagram of an nP heterojunction in thermal equilibrium.

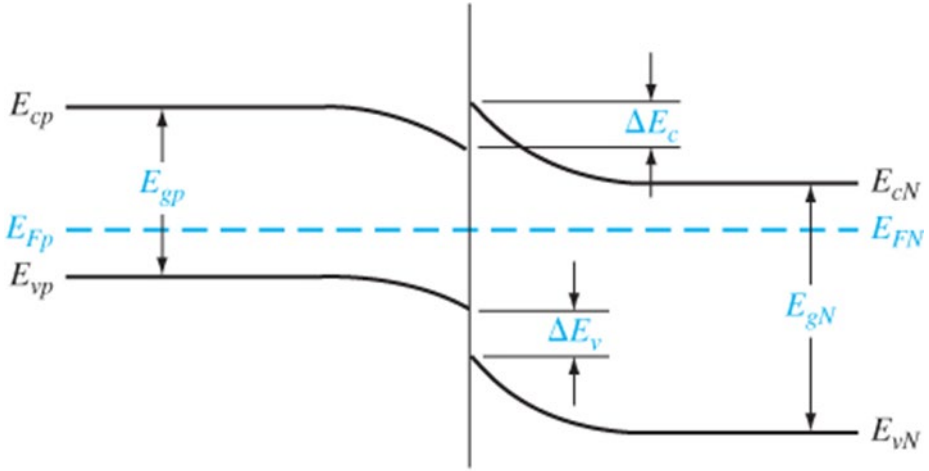

Figure 9.23 | Ideal energy-band diagram of an Np heterojunction in thermal equilibrium.

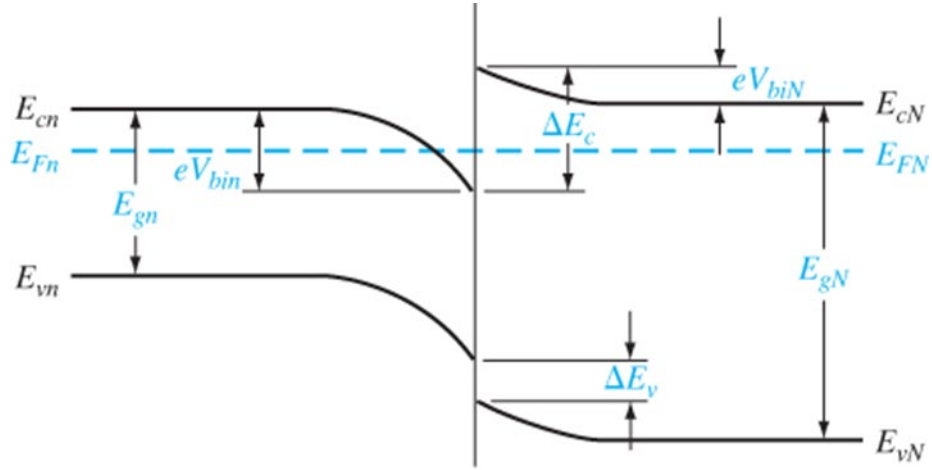

Figure 9.19 | Ideal energy-band diagram of an nN heterojunction in thermal equilibrium.

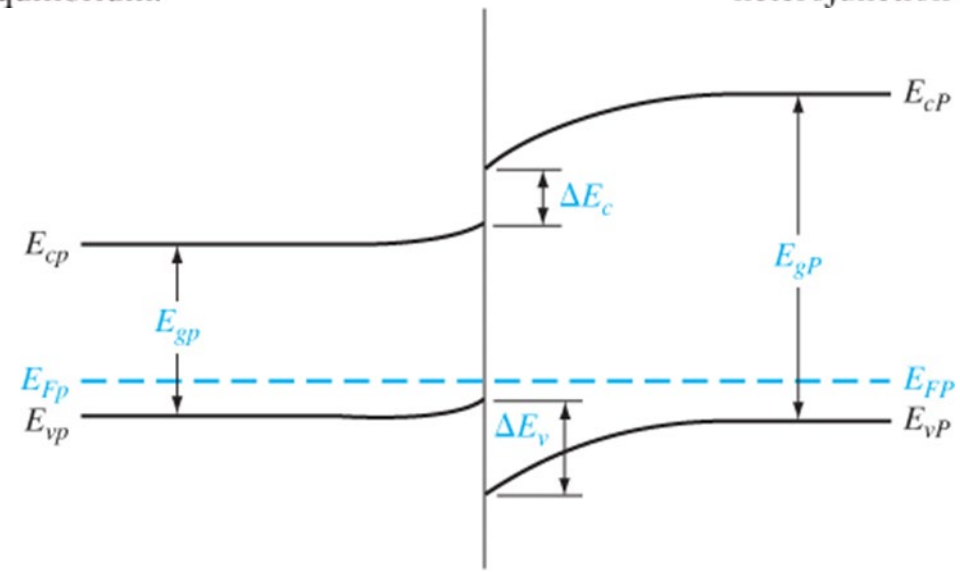

Figure 9.24 | Ideal energy-band diagram of a pP heterojunction in thermal equilibrium.

Light Propagation (Electromagnetic Wave)

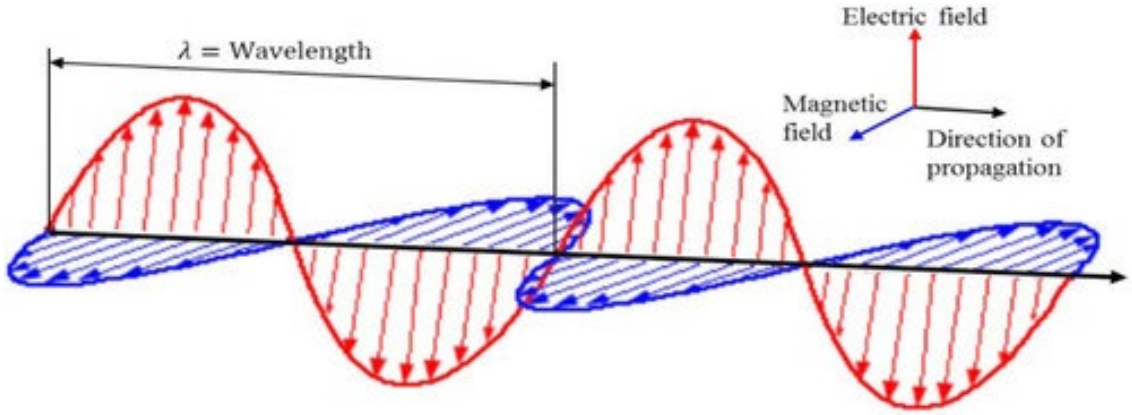

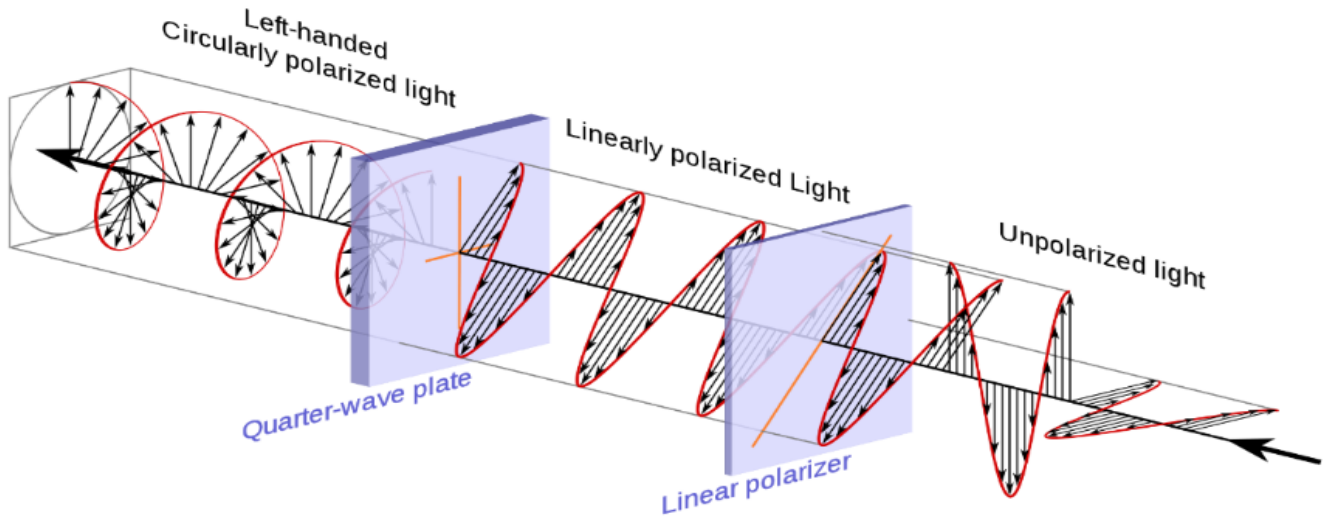

Semiconductor Bandgap vs. Lattice Contact

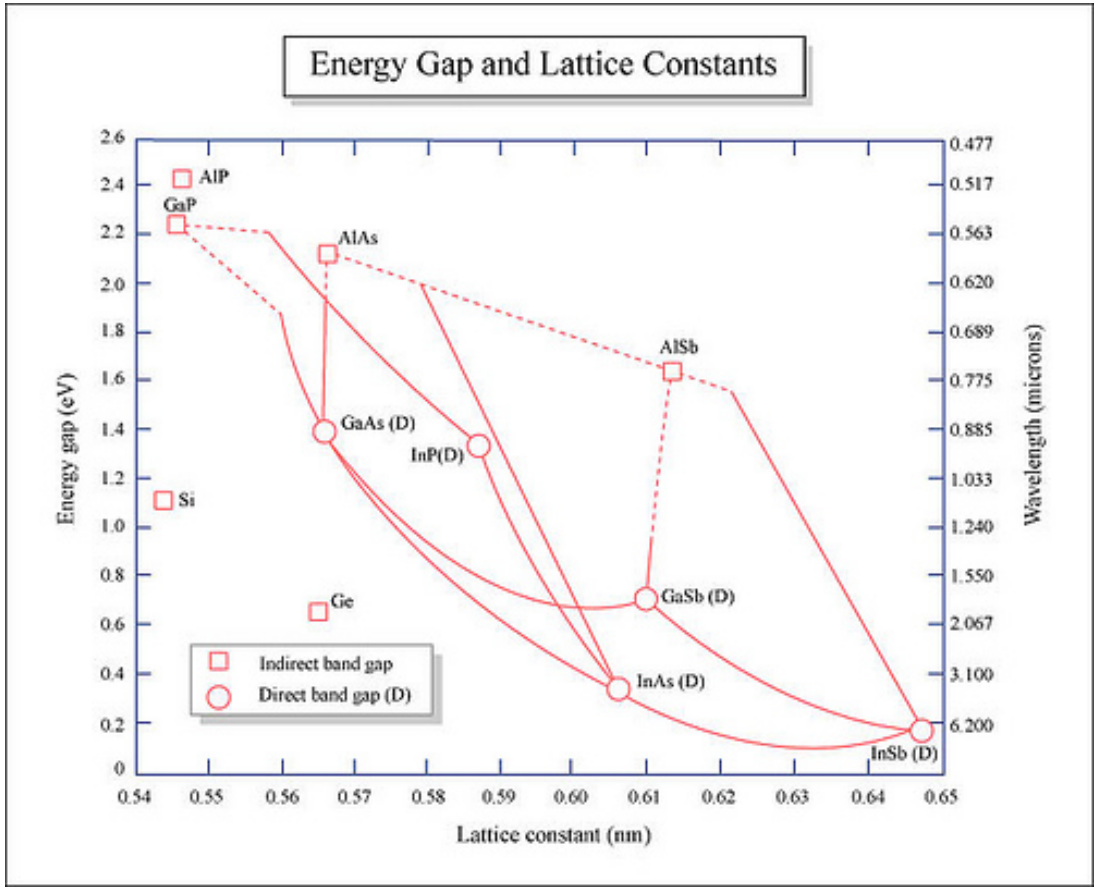

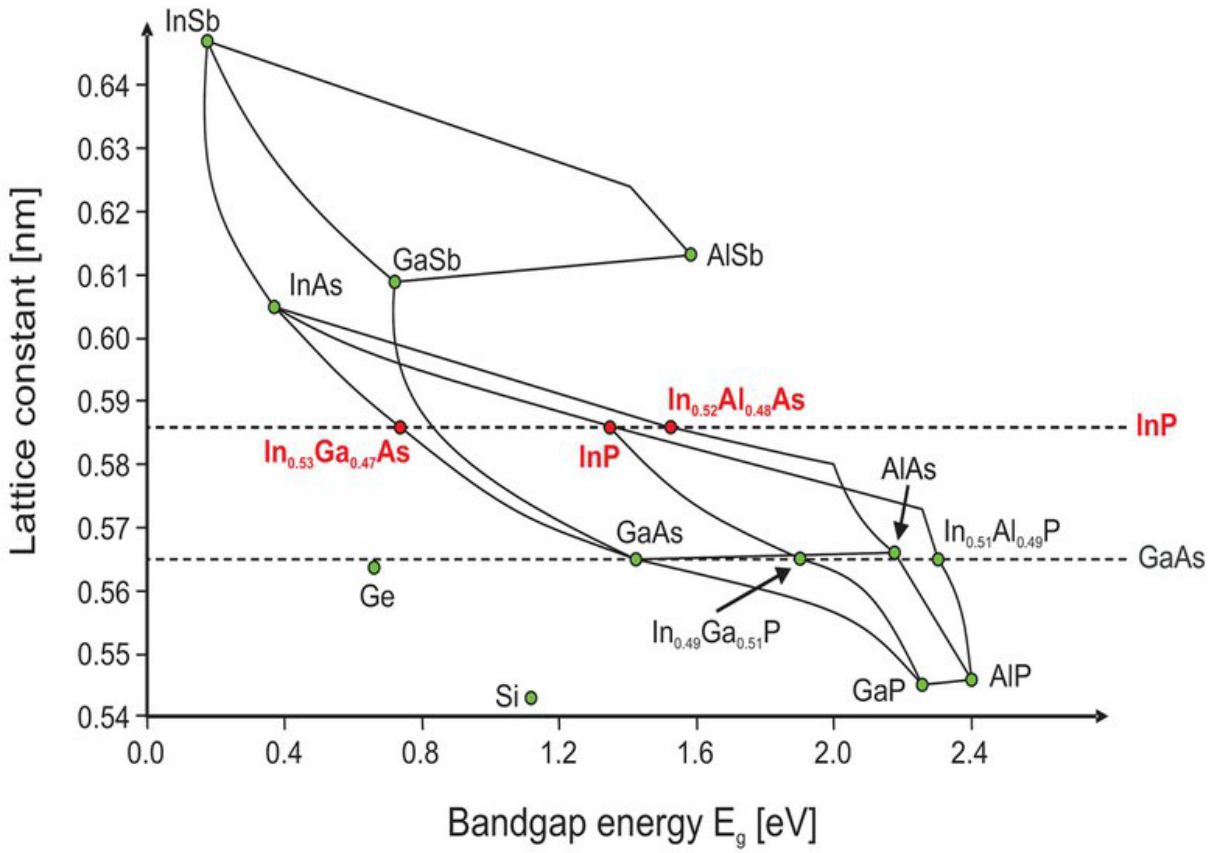

Light Absorption in SC

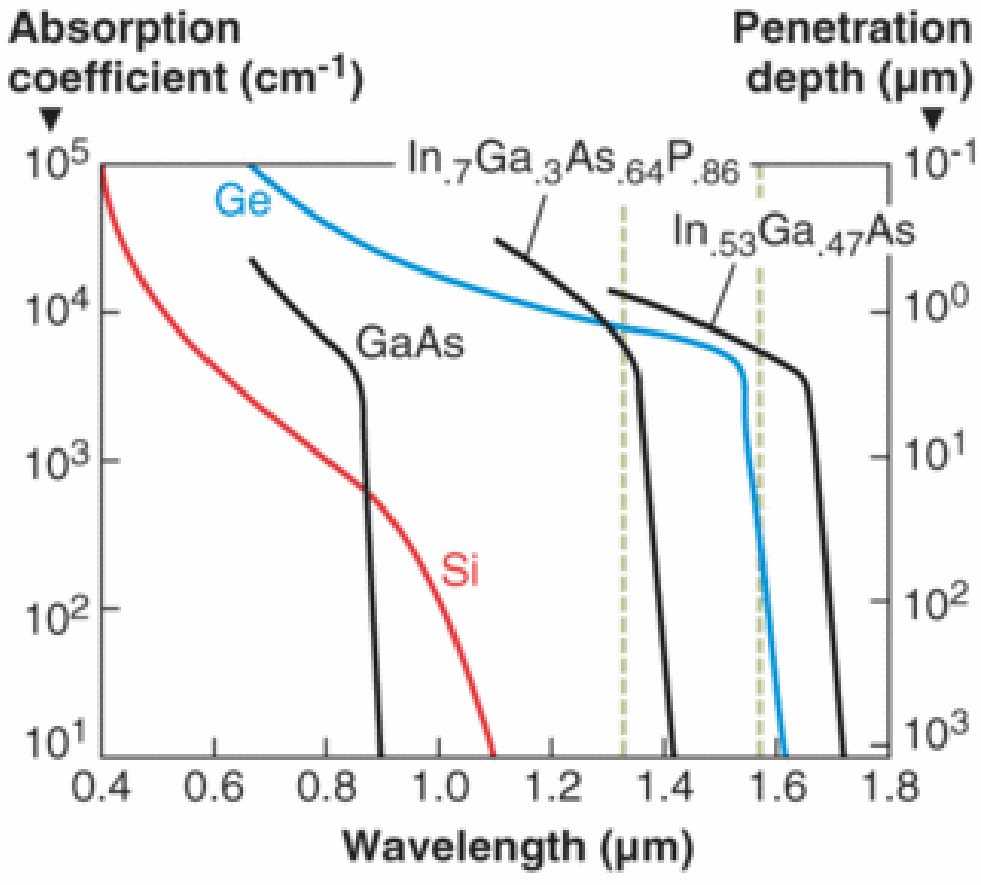

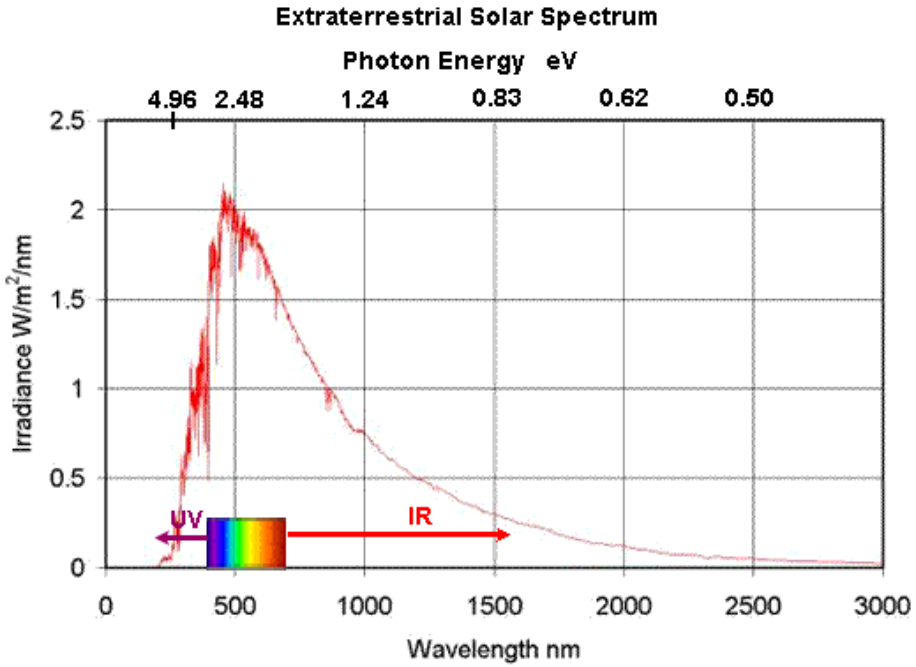
Extraterrestrial Solar Spectrum
Photon Energy eV
4.96 2.48 1.24 0.83 0.62 0.50
Irradiance W/m²/nm
2.5
2
1.5
1
0.5
0
UV
IR
0 500 1000 1500 2000 2500 3000
Wavelength nm

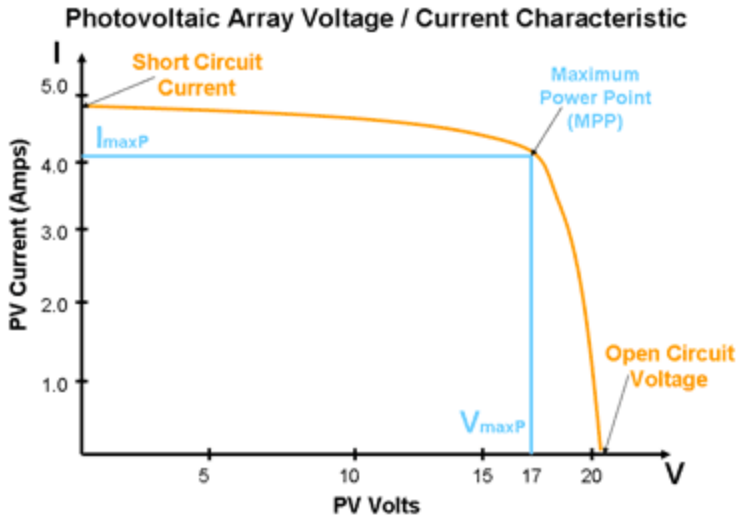
Photovoltaic Array Voltage / Current Characteristic
I
Short Circuit Current
Maximum Power Point (MPP)
ImaxP
PV Current (Amps)
5.0
4.0
3.0
2.0
1.0
Open Circuit Voltage
VmaxP
5 10 15 17 20 V
PV Volts

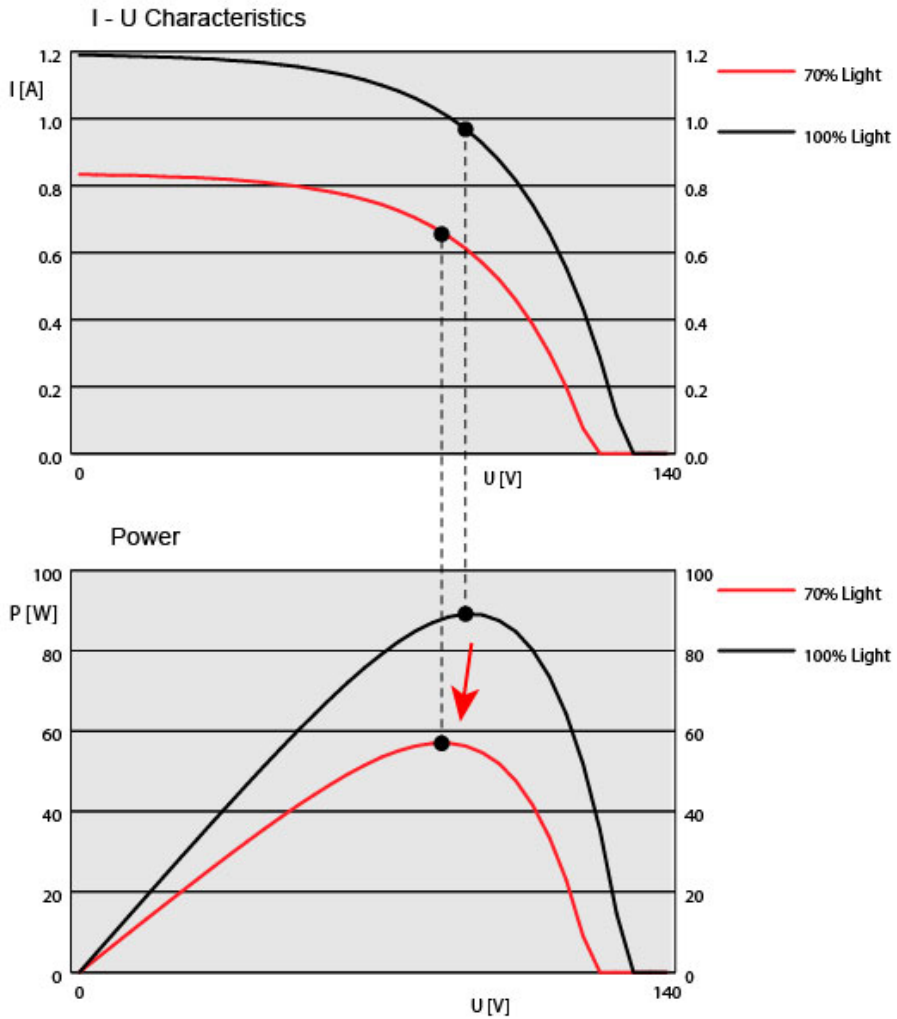
I - U Characteristics
I [A]
1.2
1.0
0.8
0.6
0.4
0.2
0.0
0
U [V]
140
70% Light
100% Light
Power
P [W]
100
80
60
40
20
0
0
U [V]
140
70% Light
100% Light

Best Research-Cell Efficiencies

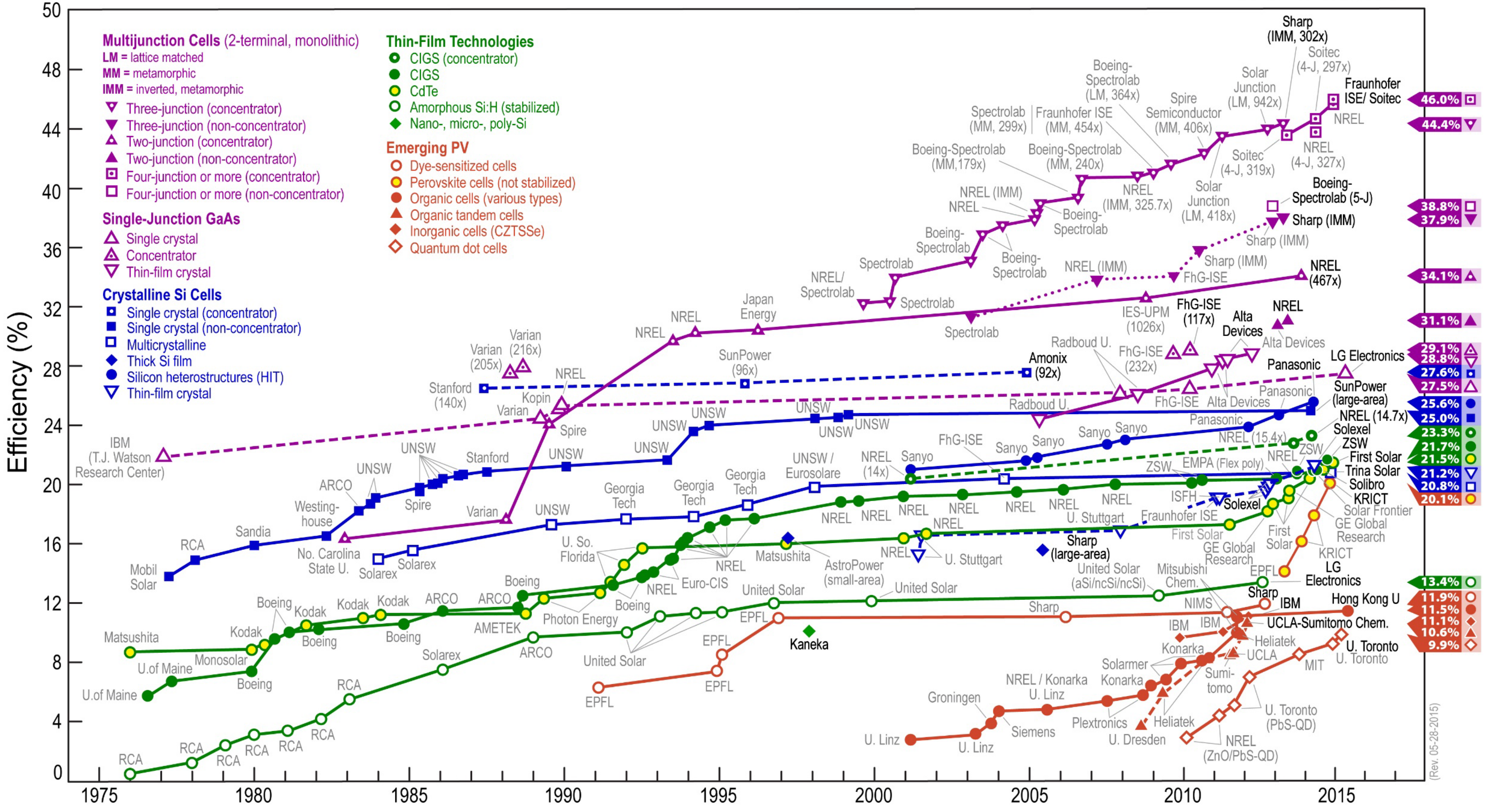

Photodiode Operation

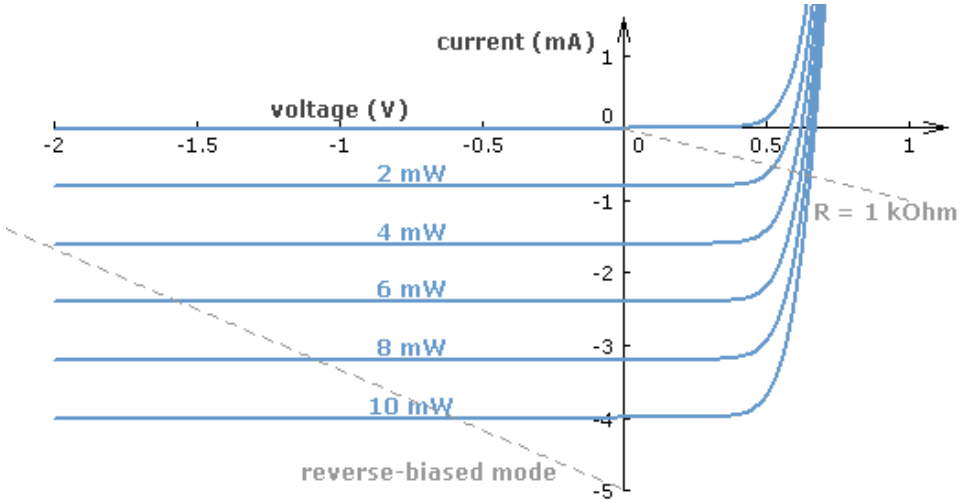

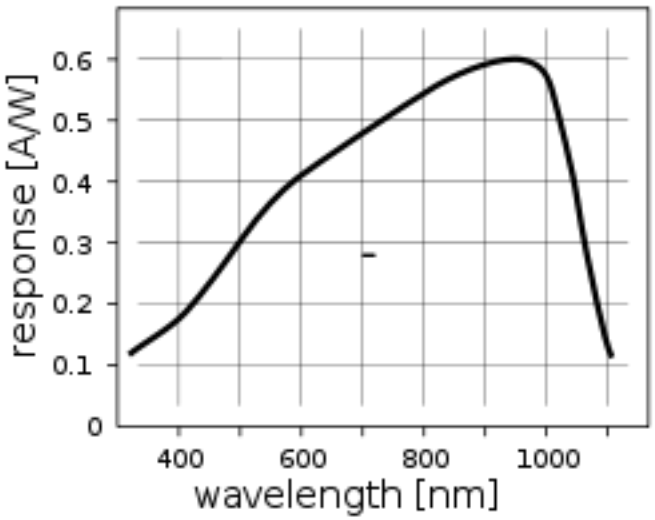

LED

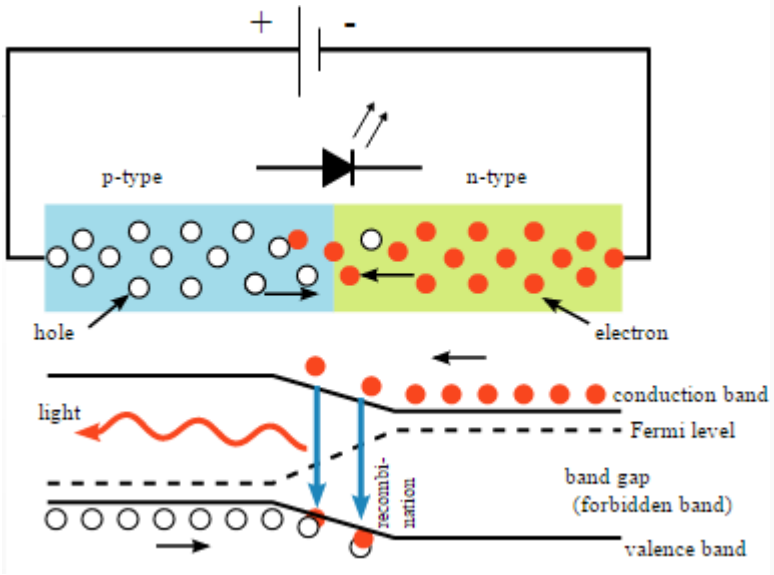

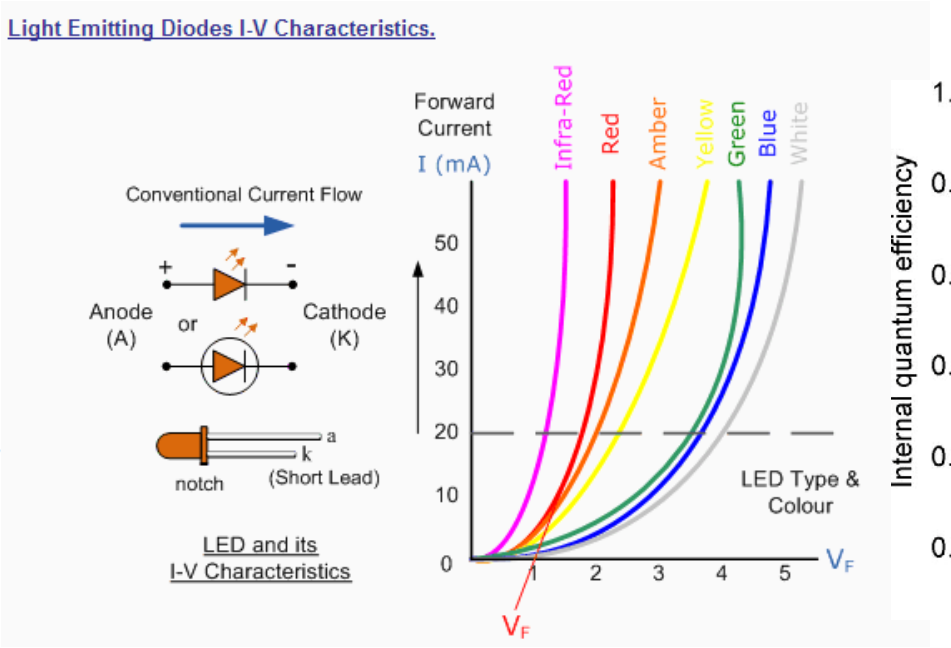

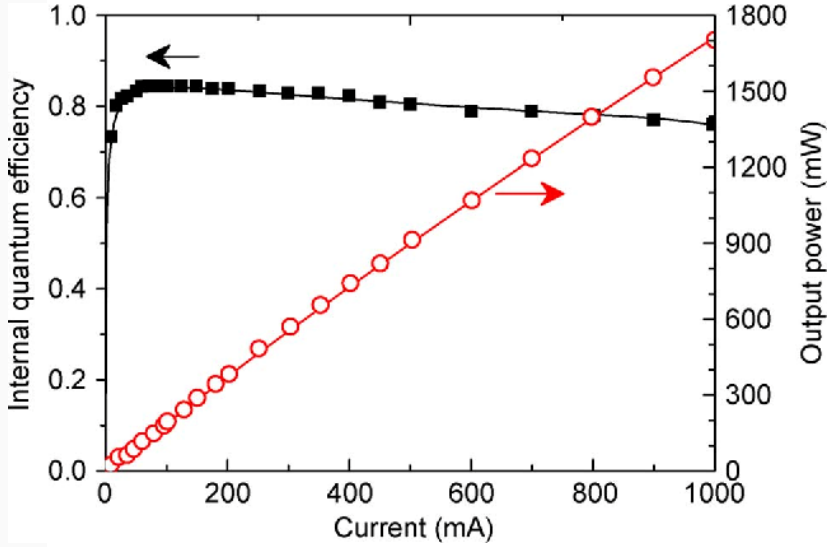

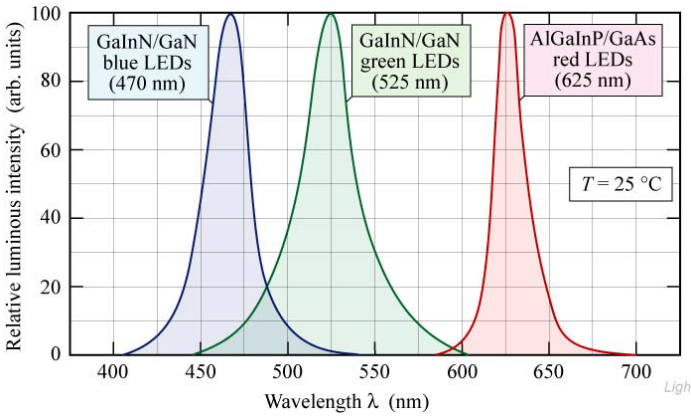

Fig. 12.16. Typical emission spectrum of GaInN/GaN blue, GaInN/GaN green, and AlGaInP/GaAs red LEDs at room temperature (after Toyoda Gosei Corp., 2000).

E. F. Schubert
Light-Emitting Diodes (Cambridge Univ. Press)
www.LightEmittingDiodes.org

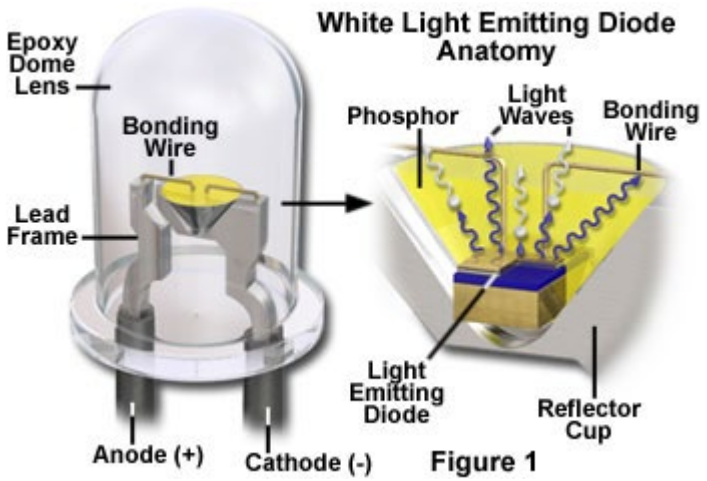

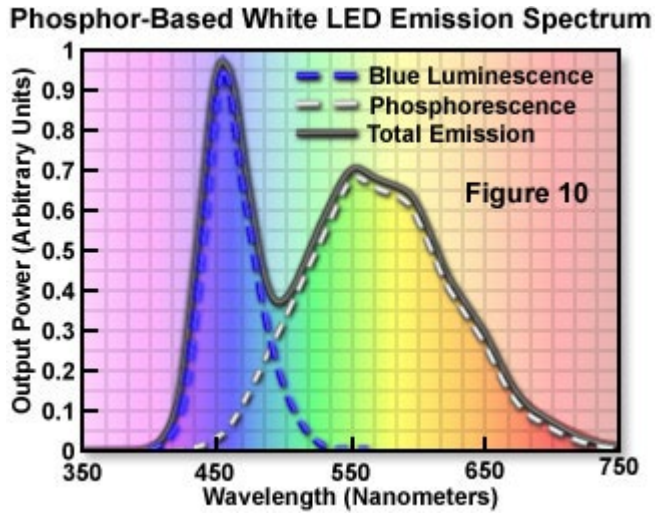

Various SC Lasers

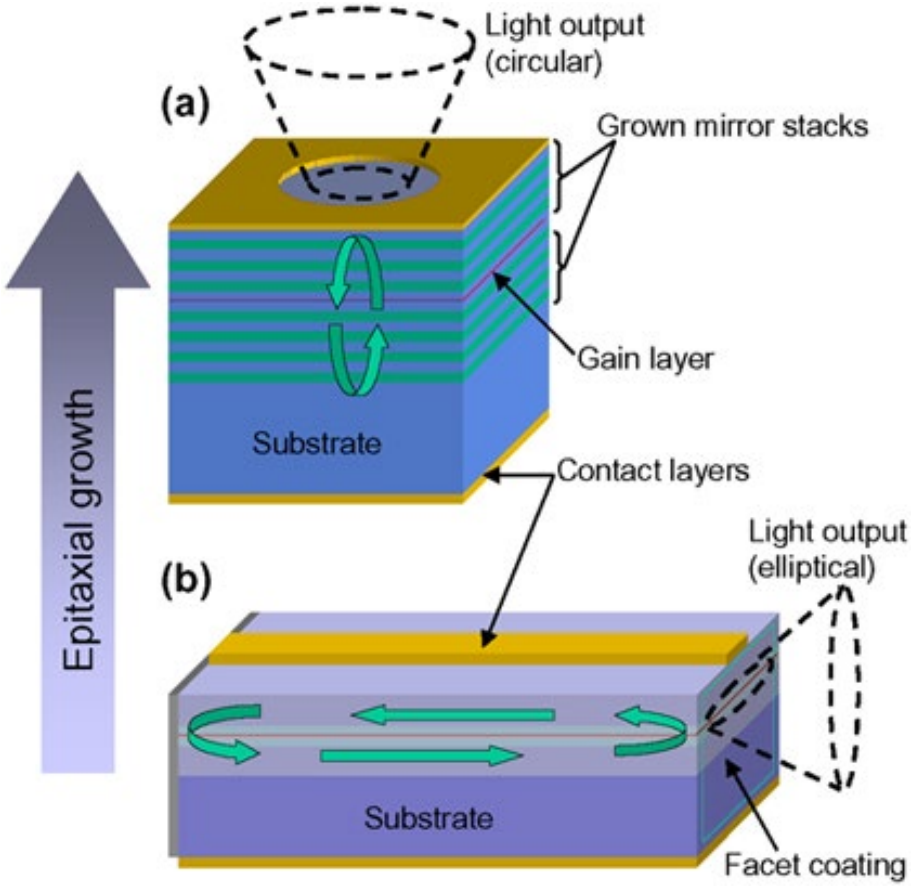

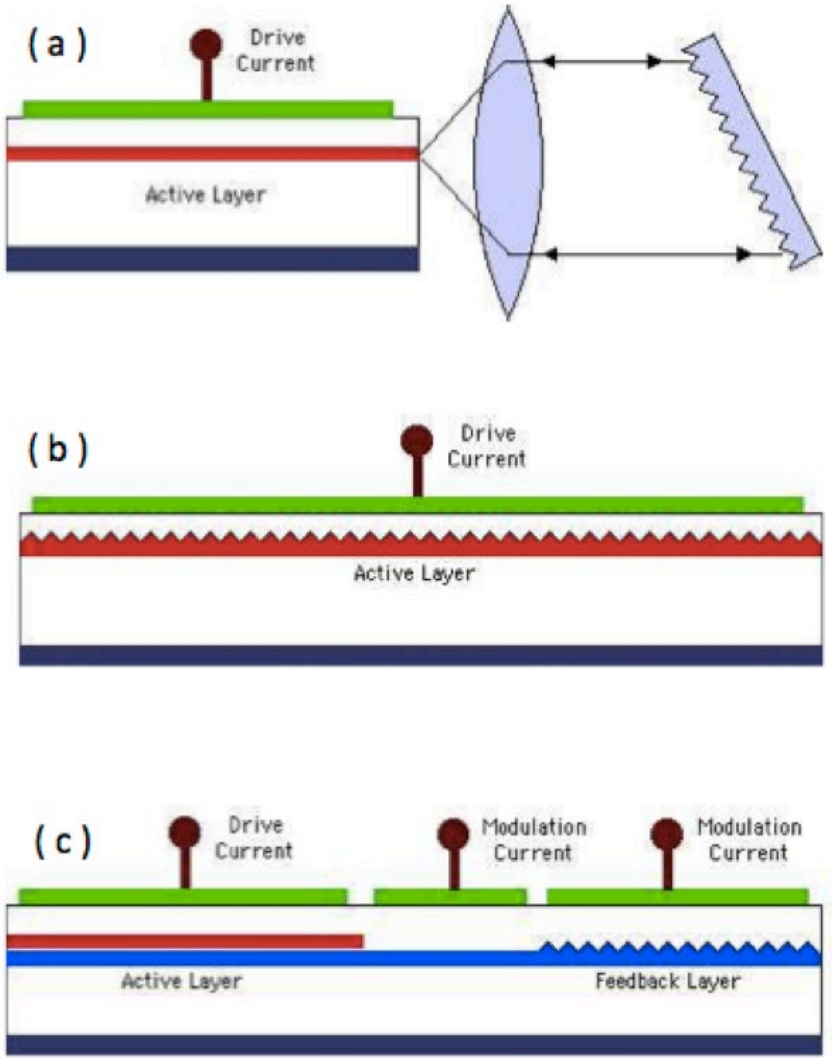

Fresnel Reflection